ABSTRACT

LEWIS, JAMAL SANA. Microstructural, Mechanical and Antibacterial Characterization of Nanocrystalline Diamond Films. (Under the direction of Roger J. Narayan.)

Nanocrystalline diamond thin films exhibit unusual hardness, wear resistance, and corrosion resistance properties, and are currently being considered for use in orthopaedic, ophthalmic, and other medical implants. The purpose of this study was to evaluate the hardness, Young's modulus, microscratch adhesion, and antimicrobial properties of nanocrystalline diamond thin films. Microwave plasma enhanced chemical vapor deposition (MPCVD) was used to deposit nanocrystalline diamond thin films on p-type silicon wafers. Raman spectroscopy, scanning electron microscopy (SEM), and high resolution transmission electron microscopy (HRTEM) were used to determine quality and phase purity of the nanocrystalline diamond thin films. The thin films consisted of diamond nodules that varied in morphology (size=60-600 nm). HRTEM showed that the films contained rectangular crystallites with dimensions between 2 – 4 nm. Raman spectroscopy confirmed that the thin film sample contained both tetrahedrally-bonded and amorphous carbon phases. The hardness and Young's modulus values for the nanocrystalline diamond thin films were 29.4 ± 11.9 GPa to 72.0 ± 10.7 GPa and 346.4 ± 98 GPa to 551.8 ± 71.5 GPa, respectively. Microscratch adhesion testing was performed on the nanocrystalline diamond films to examine the functional adhesion strength between the diamond films and the silicon substrates. The nanocrystalline diamond/silicon wafer systems demonstrated very good film adhesion ($L_{CN} \approx 3.1 – 3.4$ N). A CDC biofilm reactor was utilized to incubate and grow *Pseudomonas fluorescens* on the surfaces of the nanocrystalline diamond thin films and stainless steel coupons. Quantitative data showed that bacterial attachment on the nanocrystalline diamond thin

films was quite significant and comparable to that on stainless steel surfaces. This work suggests that nanocrystalline diamond thin films are good candidate materials for biomedical implants but are susceptible to microbial colonization.

MICROSTRUCTURAL, MECHANICAL AND ANTIBACTERIAL CHARACTERIZATION OF NANOCRYSTALLINE DIAMOND THIN FILMS

By
JAMAL SANA LEWIS

A thesis submitted to the Graduate Faculty of

North Carolina State University

In partial fulfillment of the

Requirements for the degree of

Master of Science

Biomedical Engineering

Raleigh, NC

January 2007

Approved by:

Dr. R. Narayan
(Committee Chair)

Dr. P. Mente

Dr. A. Banes

BIOGRAPHY

Jamal Sana Lewis was born on the 7th August, 1984 in New Amsterdam, Guyana to Dawn and Leslie Lewis. He was raised in Georgetown, Guyana until he was 12 years old when he and his family moved to Kingston, Jamaica. In Kingston, Jamal attended the Wolmer's Boys' School. He graduated from Wolmer's in 2001 and began his Bachelor's of Science in Chemical Engineering. Jamal completed his undergraduate in six semesters at Florida A&M University. In January 2005, he relocated to Raleigh, North Carolina and began reading for a Master of Science in Biomedical Engineering.

TABLE OF CONTENTS

LIST OF FIGURES

Page

LIST OF TABLES

I. INTRODUCTION

The prevalence of bacterial infections in patients increases as surgical use and implantation of synthetic materials *in vivo* becomes more popular in operating rooms worldwide. The occurrence of nosocomial infections in patients with implanted biomaterial devices is quite high. For prosthetic grafts, the rate of bacterial infection ranges from 0.5 – 5% [3], whereas the observed incidence for embedded urinary catheters is even higher at approximately 30% of all urinary tract infections in the US [4]. Furthermore the high mortality rates associated with infection of these biomaterial implants is disturbing. Traditionally, this problem has been treated by high systemic dosage of antibiotic cocktails but this has proven to be limited in combating nosocomial infections. Consequently, removal of the device in conjunction with antibiotic therapy is often the only alternative remedy.

Bacterial strains are thought to be resistant to systemic prophylaxis because of a combination of physio-chemical and biological factors but mainly due to the formation of a “biofilm” layer secreted by the bacteria which protects it from the host’s immune response and decreases its susceptibility to antibiotic drugs. Bacterial infection of implanted materials proceeds by a sequence of steps. Immediately after implantation the device is coated by native proteins such as albumin, laminin, fibronectin, collagen, and proteoglycans and other organic matter or the conditioning film. This promotes the non-specific or specific binding of planktonic bacterial cells in the region of the implant. Once colonization of the implant surface is achieved, biofilm formation proceeds. If untreated this pathogenic invasion could lead to hematogenous spread and serious complications. Especially since the immune response system of the patient may be compromised [5, 6, 7, 8].

Scientists have recognized the necessity to develop antimicrobial methods to control and eradicate bacterial infection of biomedical implants. Methods that combat infection *in situ* offer a more efficient approach than systemic therapies. Researches have proposed embedding antimicrobial agents in local polymer matrices, immobilization of antimicrobial agents on polymer surfaces, and coating devices with bactericidal agents, silver compounds and proteins, and various anti-adhesive surface chemistries [8, 9, 10]. This project purports the use of nanocrystalline diamond (NCD) coatings.

In the past decade, interest in diamond-related materials (diamond-like carbon, micro-crystalline diamond, nanocrystalline diamond coatings) has soared due to their unique physical and mechanical properties. Diamond materials, known for their extreme hardness, good wear resistance, high corrosion resilience, smoothness and chemical unreactivity, have found many applications in tribology, microelectromechanical systems and surface acoustic wave devices [11, 12, 13]. Researchers have also begun to elicit its biological characteristics and have demonstrated that nanocrystalline diamond exhibit good biocompatibility and high thromboresistivity [14, 15, 16, 17]. These extraordinary physical and biological traits make it suitable for coating biomedical implants. Its resistivity to thrombosis has been attributed to decreased adsorption of fibrinogen and other blood plasma proteins following implantation [18]. This observation suggests that the surface microtopography of NCD coatings could also deter microbial colonization of implanted synthetic surfaces. However, extensive data on the antimicrobial nature of NCD coatings is yet to be published. My study investigates the microstructural and antibacterial properties of NCD coatings deposited by microwave plasma enhanced chemical vapor deposition (CVD) onto silicon substrates. Characterization was performed using scanning electron microscopy, transmission electron microscopy, nanoindentation, scratch adhesion testing and bacterial adhesion.

II. BACKGROUND INFORMATION

2.1 Pathogenic Infection of Biomedical Implants (Rates in the U.S.)

Over the last 50 years, sterilization and aseptic procedures at health care institutions have improved drastically. However, bacterial infection of biomedical implants still remains a major deterrent to the utility of implantable devices such as catheters, artificial prosthetics, and subcutaneous sensors. Embedded devices are responsible for over half of all nosocomial infections, with an estimate of 1 million cases per year (2004) in the United States alone [19]. The table below gives an estimate (based on figures from 2002) of the infection rates associated with implanted synthetic devices [20].

Table 1. Associated infection rates of biomedical implants.

IMPLANT	NONSOCOMIAL INFECTION RATE, %
Heart valve or joint prosthesis	2
Penile implant	3
CNS shunt	4
Cardiac pacemaker	5
External fixation pin	10
Left ventricular assist device	40

2.2 Bacteria Proliferation on Implanted Devices

The first step of infection of a medical implant by a bacterial strain is adhesion. Adhesion is a complex process involving many physio-chemical and biomolecular factors [21]. From a physio-chemical standpoint, adherence of bacterial cells to the implanted substrate is determined by the total interactions of such forces as Van der Waals Forces, Hydrophobicity/ Hydrophilicity, Lewis Acid-Bases properties and Brownian motion. Hydrophobicity in particular plays major role in bacterial cell-substrate and cell-cell attachment [21, 22].

Adhesion can be considered in three unique stages:- first, the adsorption of host proteins onto the biomaterial surface, followed by cell attachment to this adsorbed protein layer and finally cell to cell aggregation. When an artificial material is implanted *in vivo*, it immediately becomes coated with a plethora of blood and extra cellular matrix proteins – fibrinogen, fibrin, fibronectin, laminin and immunoglobulins. This protein layer is termed the "conditioning film" and is thought to be necessary for bacterial cells to stick to synthetic materials [5, 23]. The second phase transpires once bacteria are within 2 – 50 nm of the adsorbed, organic layer. Non-specific binding of bacterial cell wall and the conditioning layer occurs primarily due to physio-chemical interactions between various moieties in the two structures. Non-specific adhesion can also be as a result of substrate geometry and wedging into cavities on the irregular substrate surface [24]. This initial non-specific binding is required for the subsequent stage - specific adhesion. This attachment process is highly specific and involves recognition and binding of adhesins or ligands on the cell surface membrane to receptor sites on the conditioning film. Adhesins are specialized bacterial proteins present on the bacterial surface membrane that function as a “hook” to anchor the bacterial cell. Adhesins vary in structure but are generally categorized as either fimbrial adhesins (pili) or afimbrial adhesions. Pili tend to be longer, hair-like linkages compared to their short, monomeric afimbrial counterparts [25]. Adhesins act to reinforce the initial non-specific binding of the bacterial cell to the substrate. This entire process takes approximately 1 h after insertion. Specific attachment of the primary colonizers is the precursor for further multiplication and thence colonization of the substrate.

Biofilm formation on the implanted synthetic material proceeds with the secretion of “slime” by the adherent bacterial cell. Slime is an insoluble mixture of extra cellular polymers such as polysaccharides, proteins and DNA. Slime has a number of structural and functional implications for the maturing bacterial colony [5, 26]. The biofilm grows as secondary colonizers are recruited and primary colonizers divide to produce daughter cells. Finally, a mature bacterial colony is formed composed of various bacterial strains and embedded in a three dimensional, thick, organic matrix. This structure is quite resilient to the immune response of the host as well as systemic antibiotic therapy [27].

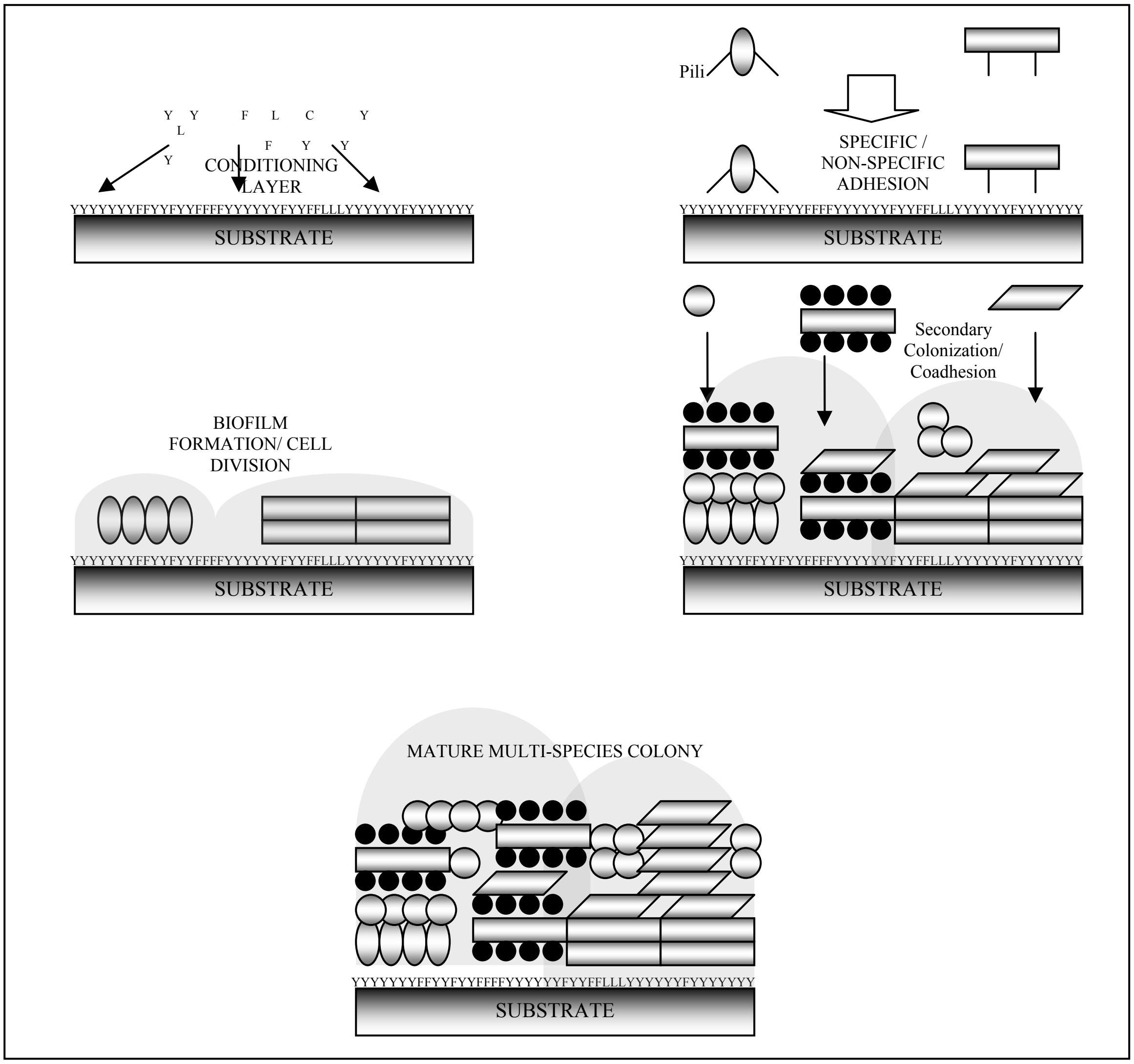

Fig. 1. Schematic of Bacterial Proliferation

2.3 Chemical Vapor Deposition (CVD)

Chemical vapor deposition (CVD) is defined as the deposition of a solid onto a heated surface by a chemical reaction in the gaseous state. It is categorized as a vapor transfer process which is elementary in nature. This class of processes also includes physical vapor deposition (PVD) techniques such as evaporation sputtering, ion plating and ion implantation. Chemical vapor deposition has been utilized in the manufacture of coatings, powders, fibers and monolithic components. The process has become an integral part of the semiconductor and electronic industry. It has also proven valuable in coating of tools, bearings and manufacture of other wear resistant and corrosion free parts [1].

The concept behind CVD was developed in the 1880’s and was used mainly to improve the strength of filaments by carbon and metal deposition in the production of incandescent lights. It wasn’t until the end of the Second World War that the potential of the CVD process became recognized and utilized on a large scale in the deposition and formation of coatings and free standing shapes. In the late 1970’s, the process took a major step forward with the advent of plasma enhanced CVD. Today the technology is speedily expanding as is the array of its applications especially because of its ability to coat almost any substrate. One notable benefit of this process is that it is not restricted to line of sight deposition as PVD techniques. It has more “throwing power”, and can easily coat indentations, grooves and other difficult 3D configurations. Chemical vapor deposition has a high rate of deposition and thick coatings can be readily produced. As with any complex process, CVD has its drawbacks. CVD sometimes requires temperatures in excess of 600 ^{o}C which limits the range of suitable substrates. Another weakness is the hazardous nature and toxicity of CVD chemical precursors and their by-products especially since these components are usually at a high pressure in the CVD chamber [1, 2].

Chemical vapor deposition incorporates principles from thermodynamics, plasma physics, kinetics, fluid dynamics and chemistry to engineer a process whereby a chemical reaction occurs in vapor phase and results in deposition of solid product on a heated substrate. The commons reactions used in CVD can be categorized as thermal decomposition (pyrolysis), oxidation, reduction, hydrolysis, disproportionation, carburization and nitridization. These reactions are activated thermally, by plasma exposure and using electromagnetic radiation. CVD reactions are governed by thermodynamics and kinetics i.e. the driving force for the reaction and rate at which it occurs. A reaction will only take place if, at the reaction conditions, the transfer of energy between species (free energy change of the reaction, ΔG_r) is negative. The free energy change of the reaction is based on the thermodynamic nature of the individual chemical species or specifically, the Gibbs free energy of the chemical reagents and products as given by the equation below, Eq. (1).

$$\Delta G_r^0 = \Sigma\Delta G_f^0\, products - \Sigma\Delta G_f^0\, reac\tan ts \qquad \text{Eq. (1)}$$

The Gibbs free energy is determined by the reaction conditions and calculated using the following formula Eq. (2).

$$\Delta G_r = \Delta G_f^0 + RT\ln Q \qquad \text{Eq. (2)}$$

where: $\Delta G_f^0 = \Sigma z_i^i \Delta G_{f.i}^0$

z_i	=	stoichiometric coefficient of species "i" (negative for reactants, positive for products)
$\Delta G^0_{f.i}$	=	standard free energy of formation of species "i" at temperature T
R	=	gas constant
T	=	absolute temperature
Q	=	$\Pi_i a_i^{zi}$
a_i	=	activity of species "i"

Once the reaction is feasible, we must establish its transport processes and rate characteristics for design and optimization of the CVD reactor. The transport of gaseous media in the CVD system is governed by fluid dynamics. The reactant gases are forced into the CVD reactor, where they diffuse through a boundary layer and are adsorbed onto the surface of the substrate where they react to give both gaseous and solid products. The vapor product is desorbed and diffuse away through the boundary layer. This sequence of transport of components is integral for a CVD reaction and the slowest step of the sequence limits the rate at which the reaction and solid deposition. The rate-limiting step can also be a consequence of surface kinetics and gas-phase kinetics. In terms of surface kinetics, the rate-determining step is affected by the temperature, pressure and reactant availability at the substrate surface. Through manipulation of process parameters and reactor design, the reaction and deposition rate can be explicitly controlled. Now that the constraints of the CVD reaction have been revealed, the next consideration is the mechanism of growth and microstructure of the deposit [1].

Researchers have proposed two theories to explain the phenomena of CVD deposit growth. The first has a thermodynamic basis and purports that due to difference in surface free energy and bulk free energy of the nucleus, a solid nucleus is formed from supersaturated vapor. The second takes an atomistic approach; it combines chemical bonding of solid surfaces with statistical mechanics to explain the growth observed on substrate surfaces. The experts, however, do agree that the properties of CVD films are affected by three factors – epitaxy, thermal expansion and gas precipitation. Of these three, epitaxy is of the greatest importance. It is defined as the growth of a crystalline film on a crystalline substrate with the substrate acting a seeding nucleus. Epitaxial growth occurs if and only if the lattice parameters (lattice constant and bandgap) of the crystalline film and crystalline substrate vary by less than 8%. A mismatch between the coefficients of thermal expansion (CTE) of film and substrate will also affect the properties of the deposited film. CTE disparity results in micro-cracking and spalling of the film. Gas phase precipitation occurs when the CVD reaction occurs away from the substrate surface (if gases supersaturated and at required temperature) resulting in the formation of soot. Soot can become incorporated into the crystalline film and affect the microstructure, surface roughness and adhesion of the coating [1].

If the film growth is successful, then one of the following three CVD microstructure types will result (based on reaction conditions):

a) Columnar grains with domed tops

b) Faceted columnar grains

c) Fine equiaxed grains (usually most desirable)

The microstructure of the deposit, including crystal size, varies with CVD reaction type, temperature, pressure, supersaturation and substrate quality.

CVD reactors are classified based on the method used to apply activation energy and initiate reaction. As such there are four basic types of CVD reactors:

i) Thermal – activated by temperature. Also known as “conventional CVD”.

ii) Plasma CVD

iii) Laser CVD

iv) Photo CVD

In this discussion, we focus solely on plasma CVD since this method was utilized to manufacture our samples.

Plasma CVD or plasma-enhanced CVD (PECVD) is so named because the CVD reaction is activated by plasma. As such, the reaction temperature is considerably lowered (compared to thermal CVD) and advantages arise from that main difference in technique. The concept behind plasma CVD wasn’t introduced until the late 1960’s. Scientists proposed that as the temperature of a gas was increased, atoms lost electrons and became ionized forming a mixture of positively charged ions, electrons and atoms (electrically neutral). At some critical temperature, all molecules are separated into atoms and ionized. This phenomena occurs only at elevated temperatures (>5000K). This restricts the number of viable energy sources for generating this plasma. To overcome this energy barrier, the use of low frequency discharge was proposed to achieve a high temperature. This increases the electrical energy in the fixed quantity of gas so that all molecules break apart and become charged. Electrons and ions both react to the constantly fluctuating direction of the electric field; acquire energy and their temperature is raised equally (isothermal plasma). Because this process transpires at high temperature (100 Torr to 1 atm), the average distance between molecules is less and the frequency of collision is increased; consequently molecules and ions are quickly heated. A major disadvantage of isothermal plasma is the high power requirement and high heat generation. As such, non-isothermal plasmas which require less power to be generated have been preferred for use in modern PECVD reactors. Non-isothermal plasmas are generated by high frequency electric fields and at lower temperature than isothermal plasmas. In high frequency electric fields, electrons are accelerated to high temperatures while ions due to their much greater mass are heated much slower. Consequently, the overall temperature of the plasma remains relatively low. Collisions between the high energy electrons and gas molecules derive reactive chemical species and initiate chemical reaction. High frequency currents normally used are radio frequency (RF) at 13.45 MHz and microwave (MW) frequency at 2.45 GHz. These frequencies are generated by various plasma generators such as electron cyclotron [2].

Advantages of plasma CVD over other techniques include:

i) Coating of low temperature substrates such as aluminum (melts at high temperature), organic polymers (degrade), metals or metal alloys (undesirable structural changes) and various other substances that may diffuse away when temperatures are elevated.

ii) Because of the reduced temperature, the effects of thermal expansion mismatch between the deposited film and substrate are minimized.

iii) Low temperature deposition also favors formation of very fine grained polycrystalline films which have desirable properties.

iv) Faster film growth rates.

Limitations are as follows:

i) Desorption off by-products and other gases can occasionally prove difficult and may sometimes be incorporated into the CVD film leading to undesirable properties.

ii) Fragile substrates (some semi-conductor materials) can be damaged by ion bombardment.

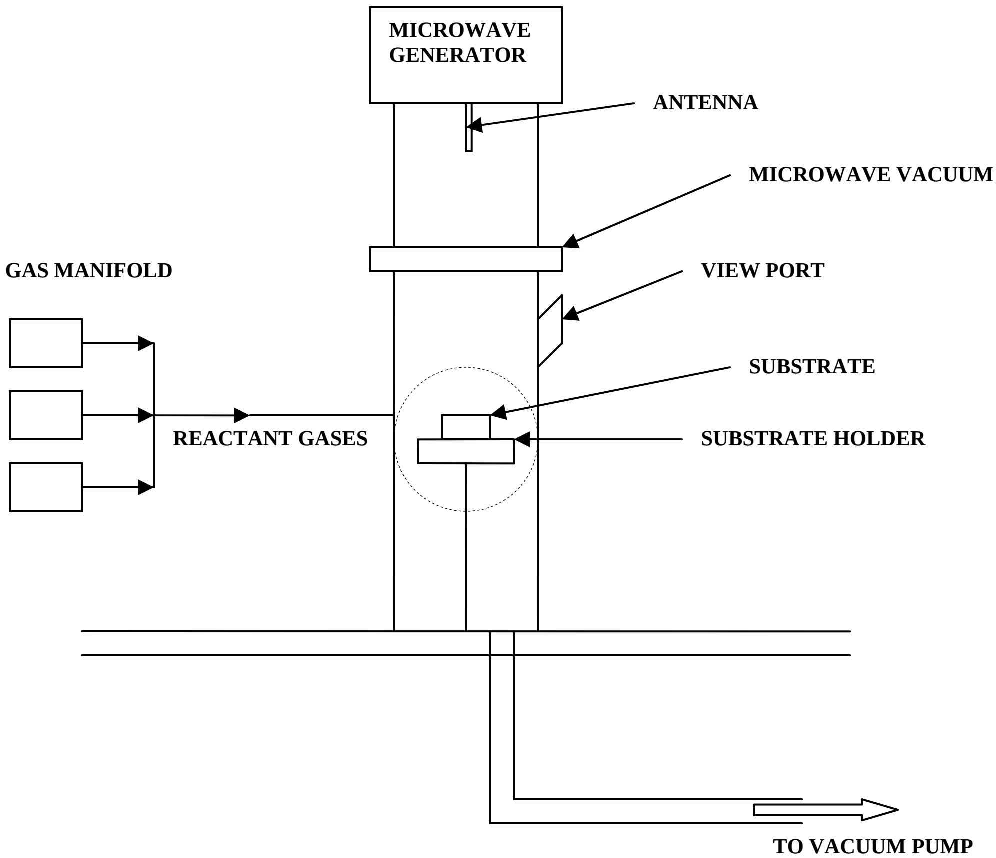

Fig. 2. Schematic Diagram of Plasma Microwave CVD Reactor

2.4 CVD Diamond

One of the tenants of thin film and coatings is the ability to impart any substrate with desired surface properties yet maintain the bulk properties of the substrate. This notion has relevance in many areas including tribology. To this end, scientists have sought to exploit the innate properties of diamond.

Diamond, first discovered in India at about 800 BC, was chiefly used as ornamental stones and as exchange currency. But today, its uses have expanded and it is being used in semiconductors, MEMS, and cutting tools. Diamond is an allotropic form of carbon with higher density than graphite and a compact structure of coordinated tetrahedral sp^3 bonds. This atomic structure of diamond accounts for its unique properties. The table below details diamonds exceptional characteristics [2].

Table 2. Properties of Diamond

DIAMOND PROPERTY	NUMERICAL VALUES	COMPARISON WITH OTHER MATERIALS
Vickers' Hardness	12000-15000 kg/mm^2	Hardest material known
Thermal Conductivity	18W/cm.^{o}C	Highest thermal conductance
Thermal Expansion	2.8 ppm/^{o}C	Close to that of SiO_2 (low)
Chemically Inert	Inert up to 600^{o}C when it oxidizes	Resistant to all acids, bases and solvents at 25^{o}C
Young's Modulus	1.2 x 10^{12} N/m^2	Highest mechanical strength
Friction Coefficient	0.1 (in air)	Low in air; lower in vacuum
Electrical Resistivity	10^{16} ohm-cm	One of the highest

Diamond can now be synthesized in a polycrystalline form by chemical vapor deposition and also by some physical vapor deposition means (poor quality) with properties similar to those of diamond. CVD techniques for synthesizing diamond films involve pyrolysis of a carbonaceous gas and simultaneous activation of the gas phase that etches nondiamond carbon phases from the growing film. These reactions require energy for initiation; as such various techniques are used to apply this energy. Each has its own advantages and drawbacks but the mostly commonly used are microwave enhanced plasma CVD, radio frequency plasma CVD, hot filament CVD, D.C. source plasma CVD and combustion flame CVD. Hydrocarbon-Hydrogen gas mixtures typically consisting of 99% hydrogen and 1 % methane are used for CVD diamond film growth. The deposition mechanism is complex and still not fully understood. But, it has been theorized that gas phase hydrogen abstraction from the CH_4 leads to the methyl radical CH_3., which adsorbs on a carbon radical site also created by hydrogen abstraction from the hydrogen terminated growing diamond film [11]. Hydrogen abstraction of the remaining hydrogens on the adsorbed methyl radical results in more carbon to carbon bonding as well as the formation of the diamond lattice. Hydrogen plays a critical role in the process; it initiates the gas phase chemical kinetics, etches graphite forms and stabilizes the sp_3 dangling bonds found on the diamond surface plane.

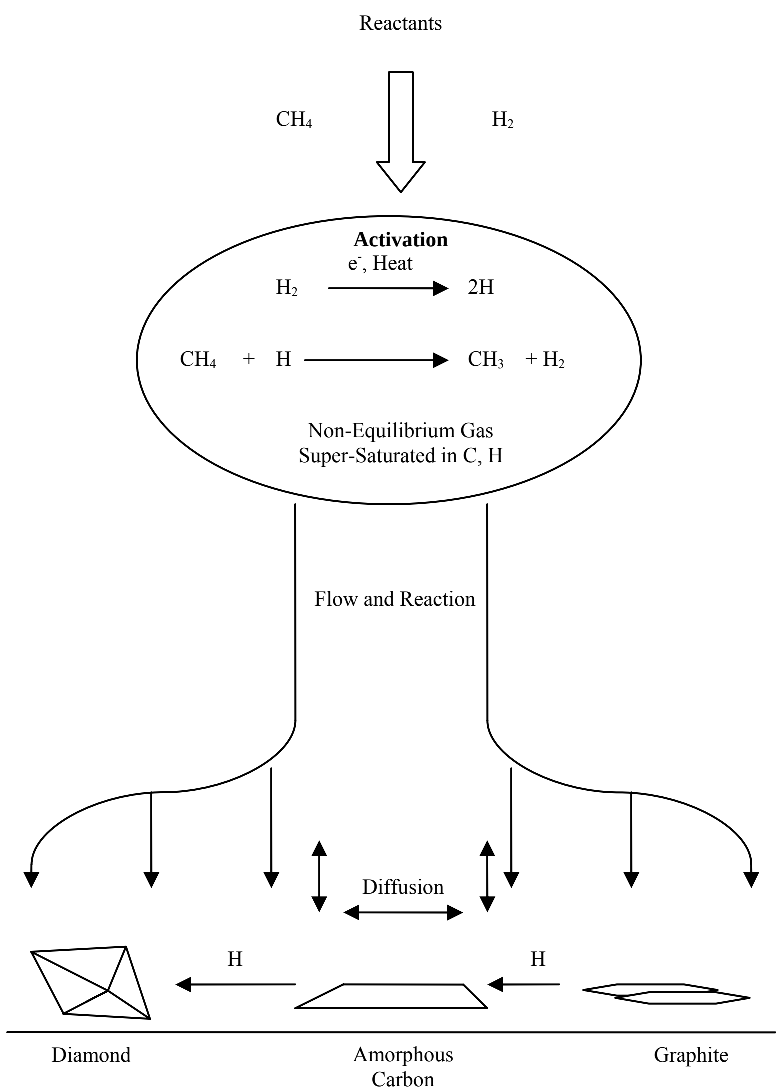

Fig. 3. Schematic Diagram of diamond CVD

2.5 Coating Characterization

Dependent on reaction conditions (temperature, pressure, reactant concentrations, substrate, etc.), there can be vast differences in the CVD film grown. It may vary in allotropic form, crystalline phase, crystal size and morphology. Thence, there has to be methods to evaluate the quality of the CVD film. Typically, scanning electron microscopy (SEM) and transmission electron microscopy (TEM) are used to discern the crystalline morphology due to their high spatial resolution (≈ 0.2 nm) in imaging and high sensitivity in spectroscopic mode. Either x-ray or electron diffraction is employed to identify the phase composition of the nanodiamond film. Techniques such as selected-area electron diffraction (SAED), electron energy-loss spectroscopy (EELS) and x-ray photoelectron spectroscopy (XPS) are also utilized for this purpose [11]. The third marker that indicates nanodiamond has been obtained is a sharp peak at 1332 cm^{-1} on a laser Raman spectrum. Raman spectroscopy is an excellent tool for identifying CVD diamond phase purity based on the peak positions on spectra. Table 3 below gives a summary of the carbon phase and its attributed peak positions [28].

Table 3. Raman spectra bands for various carbon phases

CARBON PHASE	**RAMAN SPECTRUM PEAK POSITION (cm^{-1})**
Microcrystalline Diamond	1332
	1150
Polycrystalline Graphite	1580 (G peak)
	1357 (D peak)
Amorphous Carbon	1200
	1300
	1470

In addition to these physical and chemical characterizations of the NCD coatings, nanoindentation and scratch adhesion testing were performed to assess the hardness of the coatings as well as its practical adhesion to silicon.

One criterion of wear resistant biomedical implant surfaces is that they exhibit a high degree of hardness. Nanoindentation testing is exploited in this study to determine the hardness and elastic modulus of the nanocrystalline films. Indentation has long been used as a method to elucidate the intrinsic bulk properties of materials. With recent advances in micro- and nano- machining, engineers can now apply forces in the pico-newtons range and displacements of a few nanometers. This has made it possible to examine the bulk properties of more complicated materials such as thins films and porous materials [29, 30, 31].

Nanoindentation is a simple technique; it involves monitoring of the depth of an indenter tip along with the load applied to that tip. A load-penetration curve (*F-h* curve) is generated from which the mechanical properties of the sample material are extracted.

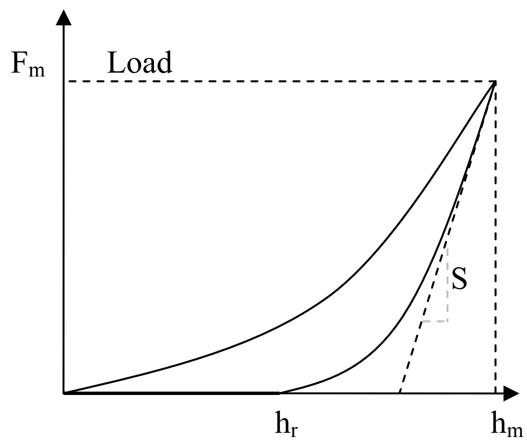

Fig.4. Loading-unloading *F-h* curves

Indenters are differentiated into two classes; sharp and spherical. Sharp indenters are employed for ductile materials for extraction of elastic-plastic deformation properties. While spherical tips are suited for brittle materials or more complex systems where small-strain elastic deformation is required for analysis. Sharp indenters are commonly three-faced Berkovich tips which allow for better definition of contact area (A_c= 24.5h_c) than four sided Vickers tips [31].

Oliver-Pharr method is used to determine the properties of the testing sample. Consider the unloading curve from a sharp contact can be fitted by the Oliver-Pharr method [32].

$$F = k(h - h_r)^m, 1 \le m \le 2 \qquad \text{Eq. (3)}$$

where F is the load on the indentation tip, h the penetration and h_r is the residual depth (after complete unloading). Then the contact stiffness (S = dF/dh) at maximum load is:

$$S = km(h_m - h_r)^{m-1} \qquad \text{Eq. (4)}$$

where h_m is the maximum depth of the indenter. The contact penetration h_c is calculated by:

$$h_c = \frac{h_m - \varepsilon F_m}{S} \qquad \text{Eq. (5)}$$

where h_m, F_m, and S are the maximum depth, force and stiffness and epilson ≈ 0.75 varies slightly with m. Then the hardness, H, can be calculated from:

$$H = \frac{F_m}{A_c} \qquad \text{Eq. (6)}$$

Generally the contact area, A_c, is given by:

$$A_c = 24.5h_c^2 \qquad \text{Eq. (7)}$$

But the actual contact area is often calibrated using a known silica material [32]. This technique is used to correct for faulty indenter tip shape and load-frame compliance of the system.

The elastic properties of a material can also be extracted from nanoindentation testing. The indentation modulus E^* (varies with specimen tip) is derived from:

$$S = \frac{\partial F}{\partial h} = 2\beta E^* \sqrt{\frac{A_c}{\pi}} \qquad \text{Eq. (8)}$$

where S is the stiffness at maximum penetration, A_c the contact depth, and β is a correction factor depending on the tip geometry (β = 1.034 for a Berkovich tip). The composite modulus (specimen tip) is:

$$\frac{1}{E^*} = \frac{1-v_D^2}{E_D} + \frac{1-v_S^2}{E_S} \qquad \text{Eq. (9)}$$

where E and v are the Young's modulus and Poisson ratio respectively, and D and S represent diamond and specimen respectively (E_D = 1141 GPa, v_D = 0.07). The reduced modulus E_r is then determined by:

$$\frac{1}{E_r} = \frac{1-v_S^2}{E_S} \qquad \text{Eq. 10}$$

Scratch adhesion testing is used to determine the practical adhesion strength and mechanical failure mode of hard, thin film, ceramic coatings on metal, ceramic, and polymer substrates. The adhesion strength and mechanical failure mode of a particular coating-substrate system is dependent on intricate properties of the system (hardness, fracture strength, modulus of elasticity, damage mechanisms, microstructure, etc.) and the test parameters (stylus properties, loading rate, displacement rate, etc) [33].

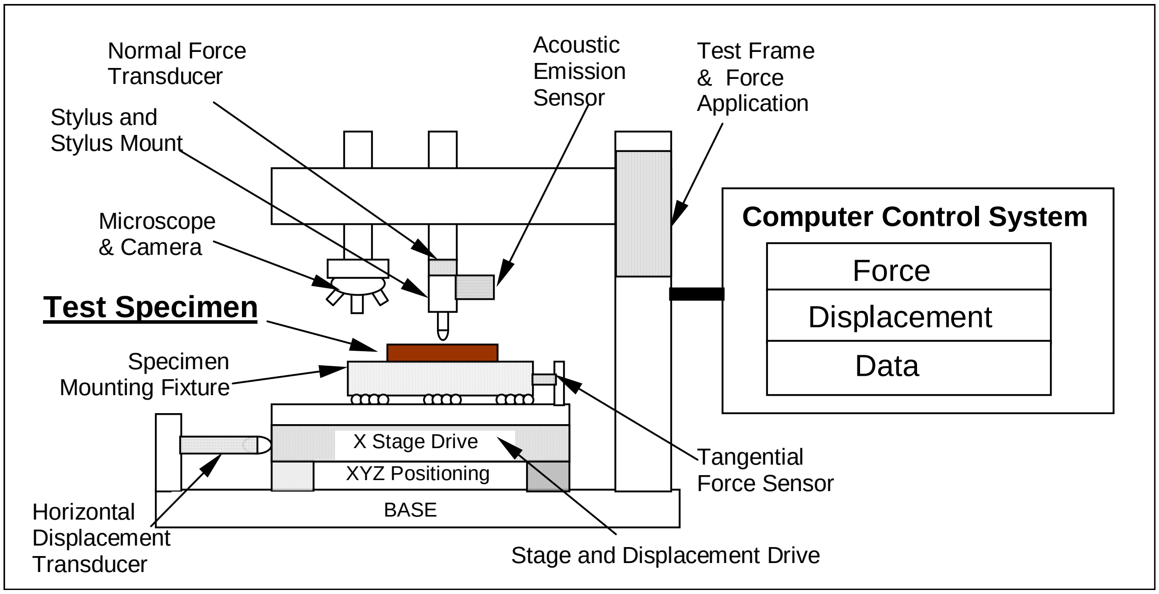

Fig. 5. Schematic of Scratch Adhesion Test Setup

Conventional scratch adhesion testing employs a diamond stylus of defined geometry and tip size to draw across the surface of the test sample a single point scratch at a preprogrammed constant speed and normal force for a defined scratch length. As the magnitude of the normal force is increased, the stylus produces progressive mechanical damage in the coating through a combination of elastic/ plastic indentation stresses, frictional forces, and residual internal stresses in the coating-substrate system. At a specific applied normal force a recognizable failure mode is observed in the coating, this normal force is known as the Critical Scratch Load (L_{CN}). The scratch adhesion test is operated in two modes; constant load scratch testing and progressive load testing. In constant load testing, the applied normal force remains at a set level throughout the test. While for progress load testing, the applied normal force is linearly increased as the test advances. Damage assessment of the coating is performed using an optical microscope commonly fitted with camera to take sequential micrographs of the scratch track.

Imaging of the scratch path is used to correlate the type of mechanical failure mode with the applied normal force. Other measurements taken to characterize the failure mechanism of the coating include the tangential force and acoustic emission.

It is important to note that this test although being relatively simple has its limitations. The principal limitation with this method is the thickness of the sample coating. Coatings with thickness' below 0.1 μm and above 30 μm are not recommended for testing with this instrument. Test parameters, specimen condition and properties also have to be rigid for valid data to be obtained. For instance, a flat coating surface is recommended for the test. If the surface is not flat, it may result in skipping, bouncing and sticking of the stylus as it draws the scratch on the specimen surface. Consequently, critical data from the test may not be recordable or legitimate [33].

2.6 CDC Bioreactor

To assess the antimicrobial nature of NCD coating, a CDC biofilm reactor was employed. This is an *in vitro* system that has been devised for cultivation of biofilms under moderate to high stress [34]. Reactor conditions are thought to mimic forces experienced by bacteria on the surface of an implanted surface better than conventional static, batch systems.

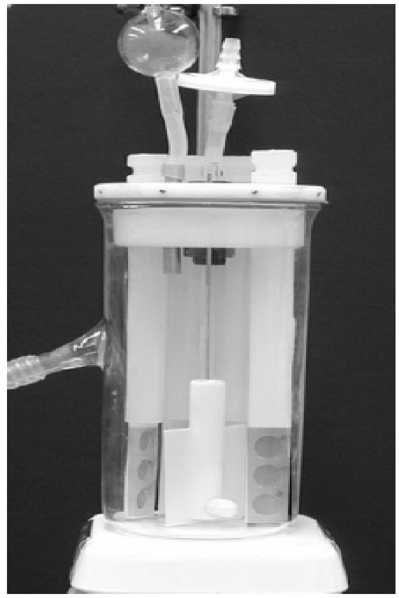

Fig. 6. CDC Biofilm Reactor

The CDC Biofilm Reactor (CBR), created by Biosurface Technologies (Boezman, MT), consists of a 1-L glass vessel encasing eight replaceable polystyrene rods that each holds three removable coupons (biofilm testing surface). Each coupon is a disk of dimensions 1.27 cm diameter and 0.3cm thick. The polystyrene rods are supported by an ultra-high molecular weight polyethylene top. The CBR is also equipped with effluent and affluent ports that allow for gaseous and nutrient exchange. The CBR is operated as a continuous-flow stirred reactor. This involves continuous passage of nutrients into and out of the CBR via inlet and outlet ports. As well as rotation of the fluid within the reactor using a baffled stir bar and digitally controlled stir plate. Rotation of the baffled stir bar not only mixes reactor fluid but introduces shear stresses to the surface of the coupons. For temperature control, the CBR is placed in a water bath. Temperature of the water bath is held constant by a digitally controlled temperature controller (Digisense, Cole Parmer) and a heating element (Heet-O-Matic, Cole Parmer) [34].

2.7 Review of Existing Literature

Implantation of medical devices is now a globally common practice in hospitals. The emergent trend of indwelling biomedical parts has given rise to an associated rate of infection from bacterial strains. The bacterial infection occurs via one of three pathways; occurrence at the wound site, contamination of the implant surface or hematogenous spread from a distant site [20, 35] Medical device infection often results in significant implant site morbidity, mortality and high healthcare costs [36, 37].

The infectious process begins with the non-specific adhesion of the bacterial strain to the implant surface via an interfacing proteinaceous layer (conditioning layer). This arrangement is guided by electrostatic forces. Specific adhesion binding by adhesin structures follows. Once bacteria has attached to the implant surface, it begins to secrete extracellular polysaccharides (biofilm) and multiply by mitosis. These steps in conjunction with the entrapment of other bacterial strains give rise to a colony on the surface of the material within a protective biofilm. Ultimately, this leads to more hematogenous spread and systemic toxicity by endotoxin release [5, 21, 22, 24, 27, 35, 38]

Bacterial infection is treated by either systemic distribution or locally dispensing antimicrobial approaches. Systemic antibiotic prophylaxis was the primary means of combating infectious disease. This method introduces antimicrobial compounds (penicillins, fluoroquinolones, cephalosporins, etc.) to the infected patient by injection into the circulatory system. In the late 1970's when it was first initiated, it was heralded as nothing short of "miraculous" for its ability to destroy staphylococcal, streptococcal and mycobacterial strains. Systemic prophylaxis proved effective in eradicating pathogens that spread via the bloodstream to sites away from the implant. However a decade later, due to generally poor effectiveness at the implant site as well as the emergence of antibiotic resistant strains of bacteria, this method was deemed insufficient against infections associated with implanted medical devices [20, 36]. The efficacy of locally administered methods was considerably higher than that of the systemic approach.

Over the twenty years, scientists have strived to develop a local antimicrobial therapy that would be clinically effective and accepted by the medical community. The earliest method was simply dipping the medical device in an antibiotic concoction. The antibiotic solution forms a clinically effective coating of the device (substrate) but the quantity of drug coated as well as the duration of delivery made this an inadequate treatment [20, 39]. Other means proposed generally came under two strategies – local drug delivery methods or coatings which rendered the device less susceptible to bacterial invasion. One of the first antimicrobial delivery systems was the silver ionotophoretic catheter developed by Raad *et al*. [40] in 1994. Utilizing the known bactericidal effects of silver ions, Raad *et al*. proposed an arrangement consisting of silver electrodes wound around the catheter from which silver ions were released once a low power was supplied. In 2002, a sustained-release system of vancomycin (VCM) using poly-L-lactide-co-caprolactone (PLCA) by Hirose *et al*. [3]. This mode provides antimicrobial compounds locally at a high dosage. The limitations associated with local delivery methods include the inability dispense antimicrobial agents at a continuously high level for long periods (months – years).

Currently the more popular route to confer immunity from bacterial infections is modification of the surface chemistry of the device. Covalent surface modification either reduces bacterial adhesion, fixes or releases bioactive molecules which are deleterious to pathogenic organisms. A number of schemes in this mode have been proposed with silver coatings being a prominent solution [41, 42, 43]. Silver coatings have for the most part failed *in vivo* because of inactivation by body fluids. Some researchers have suggested attaching biocidal moieties (quaternary ammonium salts, triclosan, fluoroquinolones) to universal biomaterials (polyurethanes, polysilicones) [4, 44]. For instance, Flemming *et al.* functionalized polyurethane with iodide containing quarternary ammonium salts. *In vitro* studies show that this surface is bactericidal to *S. Aureus*. One major drawback with this strategy is masking of the surface by proteins once implanted reduces its efficiency greatly [39]. Other chemistries seek to reduce bacterial adhesion to the implanted surface. Tsibouklis *et a.l* (1999) [8] discussed a “non-stick”, low surface energy approach (methylpropenoxyfluoroalkylsiloxanes) that prevents bacterial adhesion onto surfaces. *James et al* [4] contributed a similar anti-adhesive model in the surface thiocyanation of poly(vinyl chloride) (PVC). This method aims to disrupt the non-specific and specific binding stages of the bacterial colonization i.e. they upset the physio-chemical forces that guide the binding of substrate and microorganism. Due to the complex nature of bacteria – biomaterial interaction, it is highly unlikely that constructing a hydrophobic or hydrophilic surface will completely prevent bacterial adhesion [44]. As such, novel techniques that reduce pathogenic infection of implanted materials are still needed. This project proposes the use of nanocrystalline diamond thin films as a novel method to deter bacterial colonization of medical devices.

Diamond for many years has been known to possess superior physical and mechanical properties making it suitable for a number of applications in tribology, microelectromechanical systems and surface acoustic wave devices [11, 12, 13]. Diamond has ultra hardness, low friction coefficient, high wear resistance, chemical inertness, and a low thermal coefficient of expansion. Diamond and its related materials have found a niche in biomedical engineering due to these desirable properties. Diamond related materials (diamond-like carbon, micro- and nanocrystalline diamond) have been considered to coat various medical implants such as total joint replacements, orthopedic pins and screws, medical guidewires and heart valve replacements [18]. Nanocrystalline diamond (NCD), in particular, seems to be a very promising option for this application. Much effort is now centered on extracting the biological properties of NCD. Narayan *et al.* (2006) and Okroj *et al.* (2006) [14, 17] both proved that NCD thin films are biocompatible and thromoboresistive. These observations serve to boost NCD films' candidacy as the ideal coating for implants such as cardiovascular assist devices. Garguilo *et al* (2004) [18] suggested that the observed thromoboresistivity is due to a lack of protein (fibrinogen, fibronectin, von Williebrand factor, etc.) adsorption onto the NCD surface. Given the critical role the protein conditioning layer plays in initiating bacterial adhesion and thereby infection, Garguilo *et al.* indicate that bacterial colonization could be restricted by coating with NCD thin films. To this end, no work has shown conclusive data, although *Mitura et al (2005)* [16] mention in their study that NCD thin films maybe unfriendly to *E. Coli* strains.

This study investigates the suitability of NCD thin films as medical device coatings to reduce bacterial colonization and proliferation. To be successfully implanted into the body nanocrystalline diamond coating are required to be biocompatible, chemically stable, highly wear resistant and possess excellent adhesion to the implant (substrate) [15]. This work examines the wear resistance and scratch adhesion properties of NCD thin films on silicon (100) p-type wafers as well as the ability of this surface to reduce bacterial proliferation.

III. EXPERIMENTAL

3.1 NCD Synthesis (MPCVD)

Microwave plasma enhanced chemical vapor deposition (MPCVD) was used to grow nanocrystalline diamond (NCD) films on the silicon squares.

Silicon wafers, *p* type (100), were cut into squares of dimensions 25x25x0.5 mm^3. These wafers were cleansed and activated prior to use for diamond deposition [45]. Substrate activation entailed ultrasonic treatment with 20-40 μm diamond grit slurry for 2 h to enhance diamond augmentation. Substrates were rinsed with acetone and ethanol, and dried with N_2 gas before being placed in the MPCVD chamber. Prior to CVD, the silicon substrates were etched with hydrogen plasma for 30 min to remove the native oxide layer of the silicon. NCD coatings were deposited from mixtures of CH_4 (flow rate = 1 sccm), H_2 (flow rate = 4 - 95 sccm) and Ar (flow rate = 95 - 0 sccm). The deposition temperature and pressure were maintained at 800 ^oC and 95 Torr respectively for 5 h.

3.2 Microstructural Characterization

Examination of the surface morphology of the NCD coatings was performed using a S4000 field emission scanning electron microscope (Hitachi, Tokyo, Japan) and a 1530 thermally- assisted field emission scanning electron microscope (LEO-Carl Zeiss, Oberkochen, Germany). A G-5000 sputter coater (Electron Beam Services, Agawam, MA) was used to deliver a thin gold layer onto to NCD films. This gold layer improved SEM image quality. Thickness of the film was determined by cross-sectional SEM. Division of these values by the deposition time give the respective growth rates of the films. Grain size was measured by applying the line-intercept method to the SEM images. High-resolution images and selected area electron diffraction patterns were taken using a JEOL 2010 F scanning electron microscope outfitted with a field emission gun and Gatan Image Filter (GIF). Raman Scattering was performed using a Jobin Yvon triple monochromator system (model T 64000, Horiba Jobin Yvon Inc., Edison, NJ) fitted with an optical multichannel detector charge-coupled device (CCD) array and Olympus BX-41 microscope attachment. Raman spectra were obtained using an Ar^+ ion laser source at 514.5 nm wavelength. PeakFit software (Systat, Point Richmond, CA) was used to deduct fluorescence-related background noise from Raman spectra graphs. Peak positions were augmented by Gaussian interpolation of the Raman data.

3.3 Nanoindentation

The hardness and Young's modulus of the nanocrystalline diamond films on silicon (100) substrate was determined utilizing a Nanoindenter XP® system (MTS Instruments, Oak Ridge, TN). The samples were indented using a three-sided diamond pyramid tip and an ultra-low load indentation head. Indentations were performed using a trapezoidal loading curve with a constant loading rate of 30 mN/s. The nanohardness and Young's modulus of the materials was measured as a function of indentation depth and determined using the Oliver-Pharr Model. The tip was calibrated following the partial unloading method, and was cleaned with isopropanol between indentations.

3.4 Scratch Adhesion Testing

The adhesion of NCD coatings on Si substrate was determined using a CSM microscratch instrument (CSM Instruments, Irvine, CA). Scratch tests were performed with a linearly increasing load from 0 N to 4 N using a 20 μm diamond tip (Rockwell C geometry). The scratch length was set to 3mm and a rate of 1mm/min. A load of 1.5 N applied to the 20 μm diamond tip in contact with the NCD coating resulted in a Hertizian pressure of 34.5 GPa.

3.5 Bacterial Adhesion

Cell Culture

A rotating disc reactor CDC biofilm reactor (Biosurface Technologies, Bozeman, MT, USA) silicon and nanocrystalline diamond on silicon (100) circular samples were used for growth of bacteria. The CDC biofilm bioreactor and all operating components were autoclaved prior to the testing.

This reactor consists of a 1-l vessel with an effluent spout at approximately 400 ml, connected to a waste bottle. Continuous mixing of the bulk fluid is ensured by a magnetically driven (RET digi-visc, IKA Labortechnik, Wilmington, MA, USA) baffled stir bar. A polyethylene lid supports eight independent rods, each housing three removable circular disks. The lid also contains three stainless steel ports which allows the connection of two vent filters (Millex®-FG, Millipore, Bedford, MA, USA) and an inlet for the diluted growth medium. All materials and growth media were autoclaved prior to use. Low concentrations (1%) of Peptone-Trypticase-Yeast extract-Glucose (PTYG) media was used as the growth medium [46]. Initially, reactors were operated in batch mode for 24 h to establish the biofilms on the various substrata in 1% PTYG medium. Following the period of batch growth, the system was operated in chemostat mode by continuously pumping the 1% PTYG medium *Pseudomonas fluorescens* flow rate of 2 ml min−" for 48 h.

The *Pseudomonas fluorescens* (*Pseudomonas* strain #B252) was obtained from the Savannah River Site (SRS) Subsurface Microbial Culture Collection. It was isolated at SRS at a subsurface depth of 299 feet in the Congaree geological formation. Initial ID was determined by molecular and biochemical analysis.

Bioreactor Sampling

Coupon samples were removed at the two intervals (8 hrs and 24 hrs) together with 1 ml aliquots of media were aseptically removed. All samples were immediately frozen at -20ºC for later analysis. The bioreactor was maintained and mixed the entire test in a sterile lab hood at 25°C.

Microbial Analysis

Bacteria densities were determined by Acridine Orange Direct Counts (AODC) as previously described [46]. Bacteria densities in the Bioreactor media ranged from 2.98 x 10^5 cells/ml at Time 1 to 1.56 x 10^5 cells/ml after 24 hours in the reactor. Digital images of the stained cells on the coupons and materials were obtained using a laser confocal scanning microscope (Model LSM 310 Zeiss, Germany). Coupon samples were thawed, air dried in a sterile laminar flow hood, and then stained with 4, 6 diamidino-2-phenylindole (DAPI) to determine total microbial cells per microscopic field [47]. Images of the stained cells were obtained using a laser confocal scanning microscope (Model LSM 510 Zeiss, Germany).

IV. RESULTS AND DISCUSSION

4.1 Nanocrystalline Diamond Microstructural Characterization

The existence of nanocrystalline diamond (NCD) within the carbon films grown on silicon (100) wafers was confirmed using scanning electron microscopy (SEM), transmission electron microscopy (TEM) and Raman spectroscopy.

Table 4. Summary of Diamond Synthesized by MPCVD at given conditions

SAMPLE ID	**DEPOSITION PARAMETERS**						
	Temperature (^oC)	Ar (SCCM)	H_2 (SCCM)	CH_4 (SCCM)	Thickness (µm)	Grain size (µm)	Grain Geometry
1	700	95	4	1	3.05	0.56	Subgrains (0.1 µm)
2	900	95	4	1	2.80	0.60	Subgrains (0.1 µm)
3	600	95	4	1	2.29	0.59	Subgrains (0.1 µm)
4	800	95	4	1	3.69	0.06	Fine grains
5	500	95	4	1	1.78	0.17 x 0.5	Rice grains
6	1000	95	4	1	1.91	0.47	Square grains
7	800	95	4	1	3.82	0.0628	Fine grains

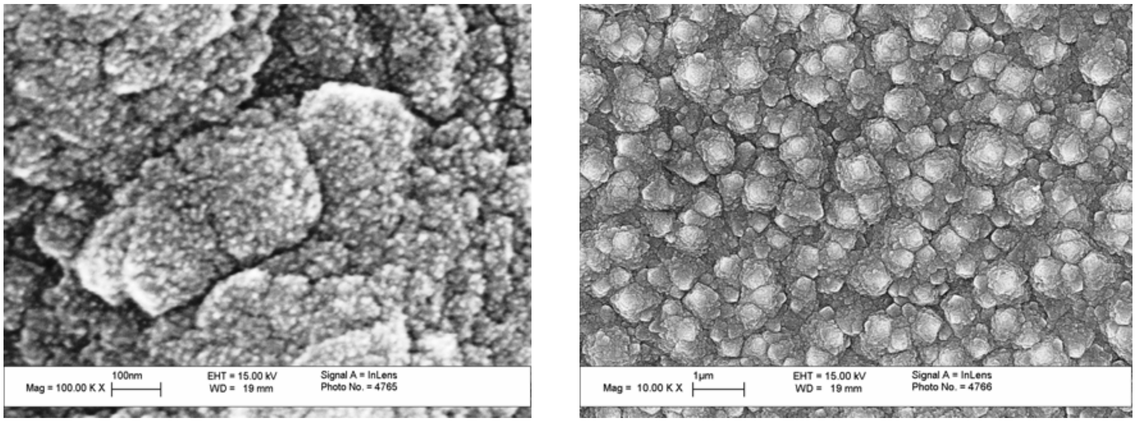

(a) x 100000 (b) x 10000

Fig 7. SEM of NCD Film on Si (100) – Sample 1

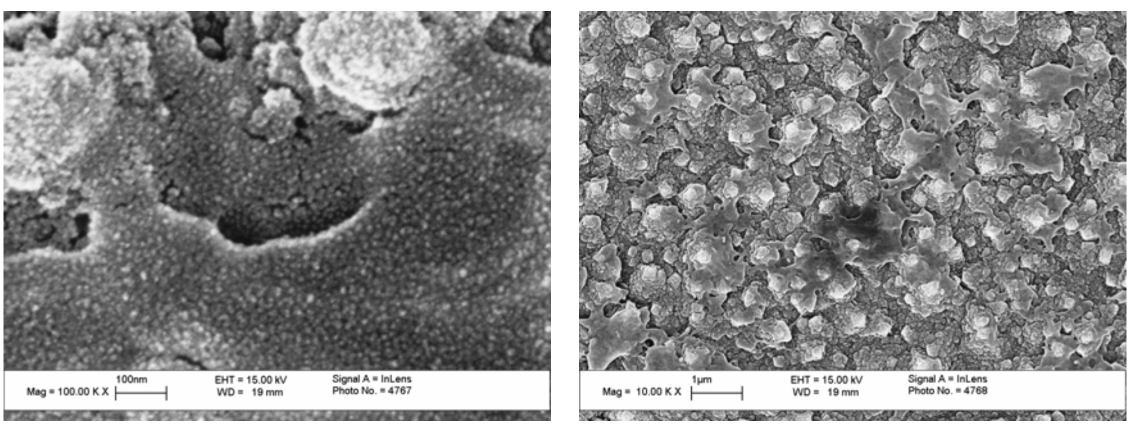

(a) x 100000 (b) x 10000

Fig 8. SEM of NCD Film on Si (100) – Sample 2

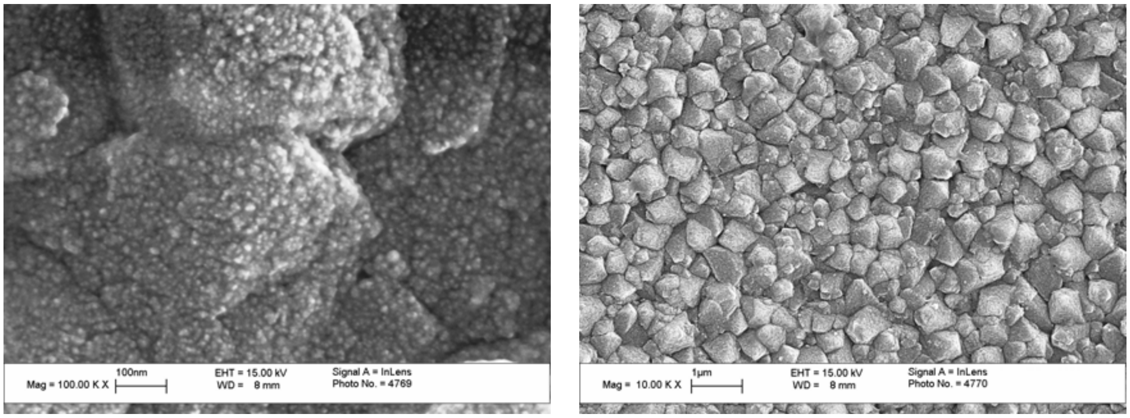

(a) x 100000 (b) x 10000

Fig. 9. SEM of NCD Film on Si (100) – Sample 3

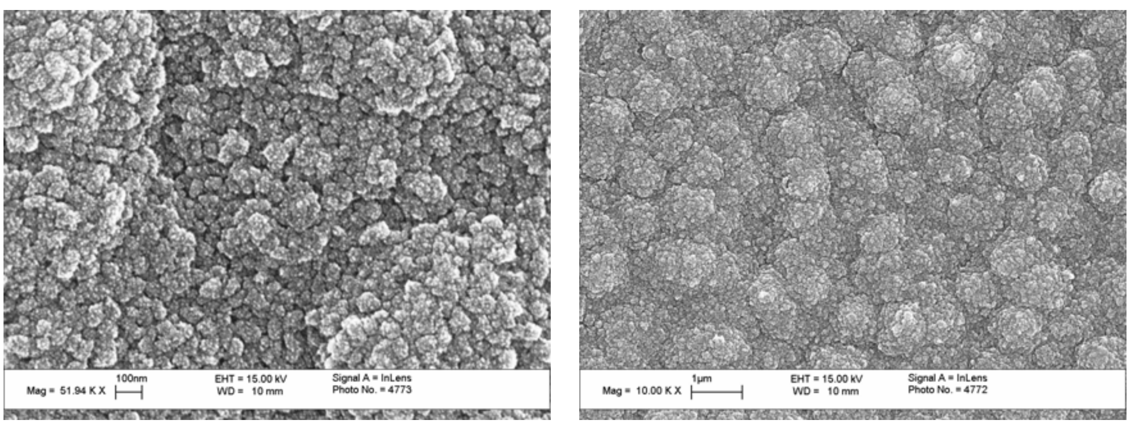

(a) x 100000 (b) x 10000

Fig. 10. SEM of NCD Film on Si (100) – Sample 4

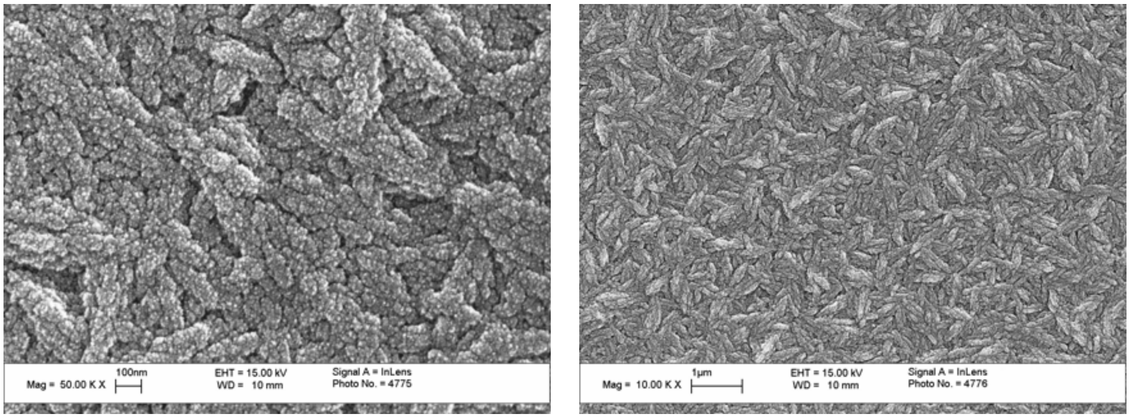

(a) x 100000 (b) x 10000

Fig. 11. SEM of NCD Film on Si (100) – Sample 5

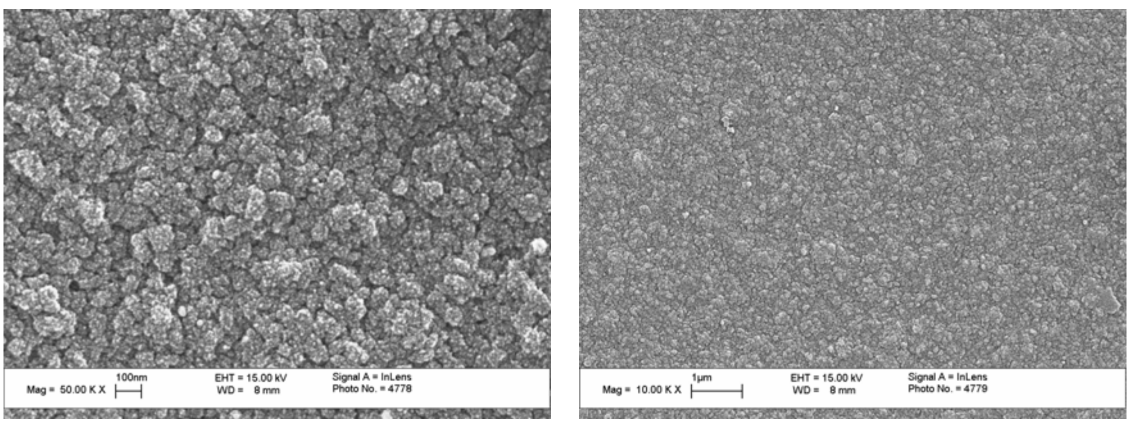

(a) x 100,000 (b) x 10,000

Fig 12. SEM of NCD Film on Si (100) – Sample 7

Different crystalline size and morphology were obtained by adjusting the temperature of the CVD reactor. SEM revealed that nanocrystalline diamond was present in the thin films grown by MPCVD. They show that the coatings consist of diamond nodules that vary in morphology and size ranging from 60 nm to 600nm with the most frequent size estimated to be 600nm. SEM images illustrate the uniformity of the NCD films over a large area for all samples contrasting to microcrystalline films that are non-uniform over the entire surface. Table 4 above gives a summary of the seven samples obtained from MPCVD nanocrystalline diamond synthesis and their characteristics based on analysis using SEM. Figures 7-12 show SEM micrographs of the NCD films at high and low magnifications for all samples except sample 6.

The size of NCD grains imparts special mechanical, electrical and optical properties in diamond films. The crystallite size is controlled by the fraction of carbon atoms residing at the grain boundaries which in turn determines crystalline grain size. The nanocrystallite size varies inversely with fraction of carbon atoms at the grain boundary [11]. Although temperatures range from 500 – 1000 ^{o}C, all films produced consisted grains with sizes less than 1μm which is an important marker for identifying nanocrystalline diamond films. A temperature of 800 ^{o}C produces the grains with the smallest diameter.

Another important observation from the SEM images is the non-rigid nodule morphology of the NCD coatings i.e. no film contained well faceted crystal grains. This implies that the coatings may contain a significant fraction of amorphous or non-sp^3 hybridized carbon atoms which is typical of NCD films [13]. This phase results from the addition of carbon dimmers instead of carbon atoms at the grain boundary. Consequently, at the grain boundaries there are heterogenous nucleation rates and bulging.

High resolution transmission electron microscopy (HRTEM) was used to determine the crystallite size of the NCD thin films. Fig. 13 illustrates the plan-view morphology of the nanocrystalline diamond coating. From these images we deduced that the nanocrystalline films have granular morphology but the sizes of the crystallites were inconclusive due to overlapping of grain boundaries in the 2D image. Closer inspection (Figs. 14 and 15) revealed that crystallites are rectangular in shape. Crystallite size is between 2 – 5 nm for our NCD thin films with grain boundaries of approximately 1 nm. This is consistent with previous studies of NCD thin films [12, 13]

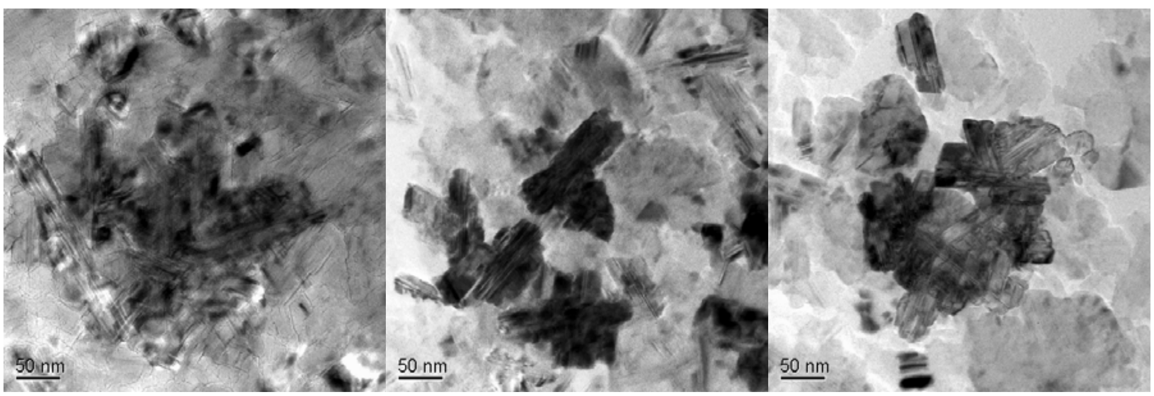

(a) Sample 2 (b) Sample 4 (c) Sample 5

Fig. 13. HRTEM of nanocrystalline diamond films x 3000

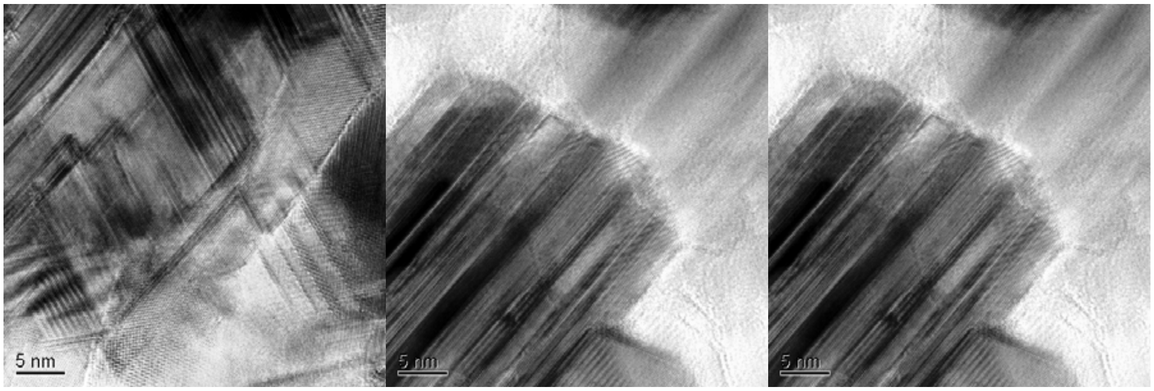

(a) Sample 2 (b) Sample 3 (c) Sample 4

Fig. 14. HRTEM of nanocrystalline diamond films x 30000

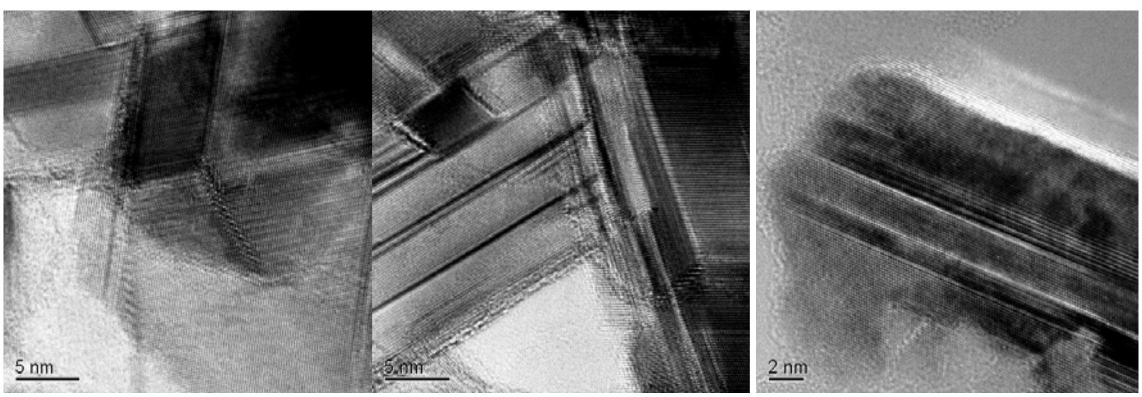

(a) Sample 1 (b) Sample 3 (c) Sample 6

Fig. 15. HRTEM of nanocrystalline diamond films x 40000

The phase purity of the nanocrystalline diamond films was examined using Raman spectroscopy. Raman spectra of the nanocrystalline diamond film samples (Fig. 16) clearly show that nanocrystalline diamond phases exist within the coatings. This is evident based on the peak observed 1332 cm^{-1} which represents carbon in a sp^3-hybridized state. The peak at approximately 1140 cm^{-1} also gives a definitive cursor to the presence of nanocrystalline diamond. This peak, often seen in nanocrystalline diamond films, has been attributed to both sp^2 – bonded carbon atoms and nanodiamond [28]. But generally, scientists assign its presence to sp^2-hybridized carbons within nanocrystalline diamond coatings with grain sizes less than 0.1 μm [48]. Additional peaks are observed at 1470 cm^{-1}, 1357 cm^{-1} and 1570 cm^{-1}. The latter two peaks are called the D and G bands respectively, giving an indication that polycrystalline graphite exists in the diamond layer. The G peak represents natural single-crystal graphite (a stretching mode of sp^2-hybridized carbon with E_{2g} symmetry) while the D peak is characteristic of a more polycrystalline structure with crystals of larger grains size (sp^2-hybridized carbon with A_{1g} symmetry) [49]. The band at 1470 cm^{-1} is attributed to the sp^2-hybridized amorphous carbon within the nanocrystalline diamond coatings. Amorphous carbon and graphite phases are frequently detected within nanocrystalline diamond films, especially given conditions at which our NCD films were grown. The sp^3-bonded carbon phase is generally increased by adding a higher percentage of H_2 in the reaction gas mixture for conventional MPCVD [28]. However; this may have an undesired effect on grain size and other properties of the film. The temperature difference also affected the final NCD content of the respective films. This is evident based on the difference in intensities observed for films 2 and 5 The Raman spectra can be used to quantify the relative amounts of NCD, amorphous carbon and graphite found in each coating by utilizing the three approaches outlined by Ramamurti *et a.l* [28]. This report does not quantify the portions of sp^2- and sp^3-hybridized carbons for two reasons. At λ = 514nm, Raman spectroscopy is fifty times more sensitive to polycrystalline graphite than nanocrystalline diamond. As such it would be erroneous to apply the method outlined by *Ramamurti and colleagues*.

Secondly, it is aim of the study to only show that there is a significant portion of sp^3-hybridized carbon within the films. This large portion of nanodiamond can be attributed to the relatively low reaction temperatures.

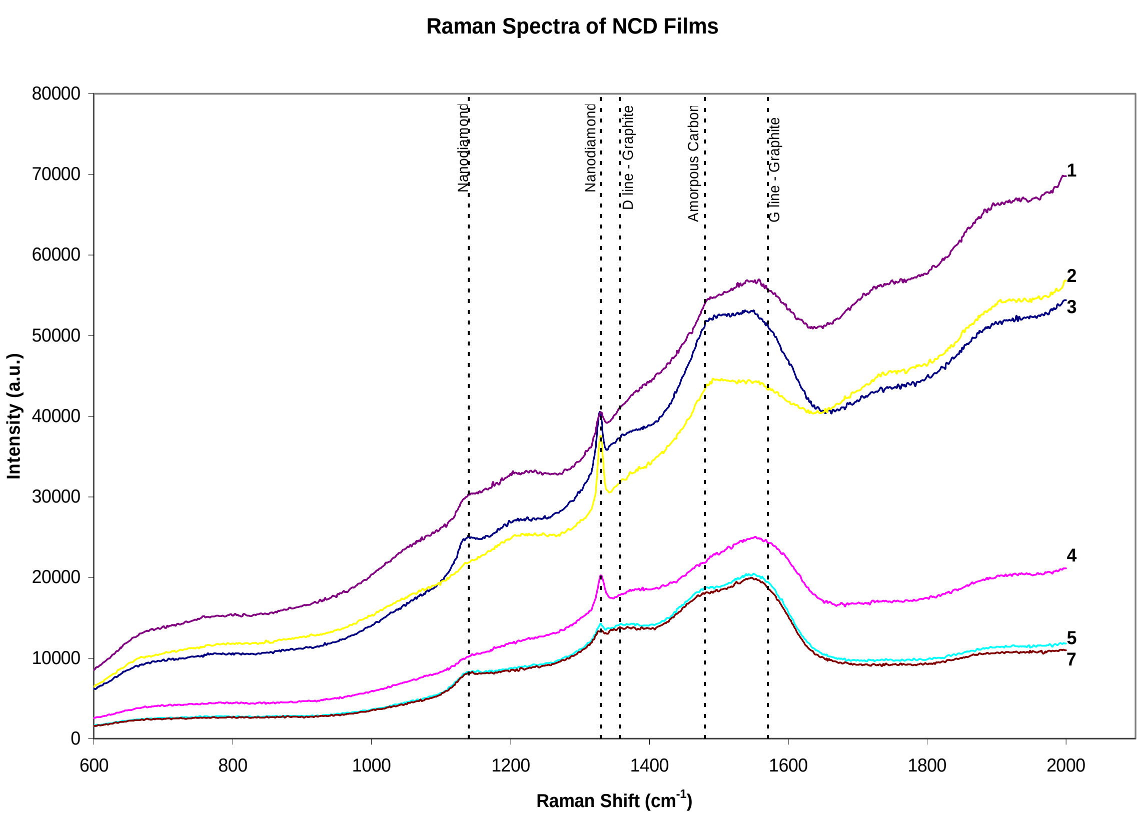

Fig. 16. Raman Spectra of NCD films deposited on Silicon (100) wafers

4.2 Nanoindentation

Fig. 17 shows the loading curves of the NCD coatings which were used to extract the hardness and indentation modulus of the nanodiamond films. These and the values for hardness and modulus of bulk diamond and nanocrystalline diamond films obtained in other studies are reported in Table. 5.

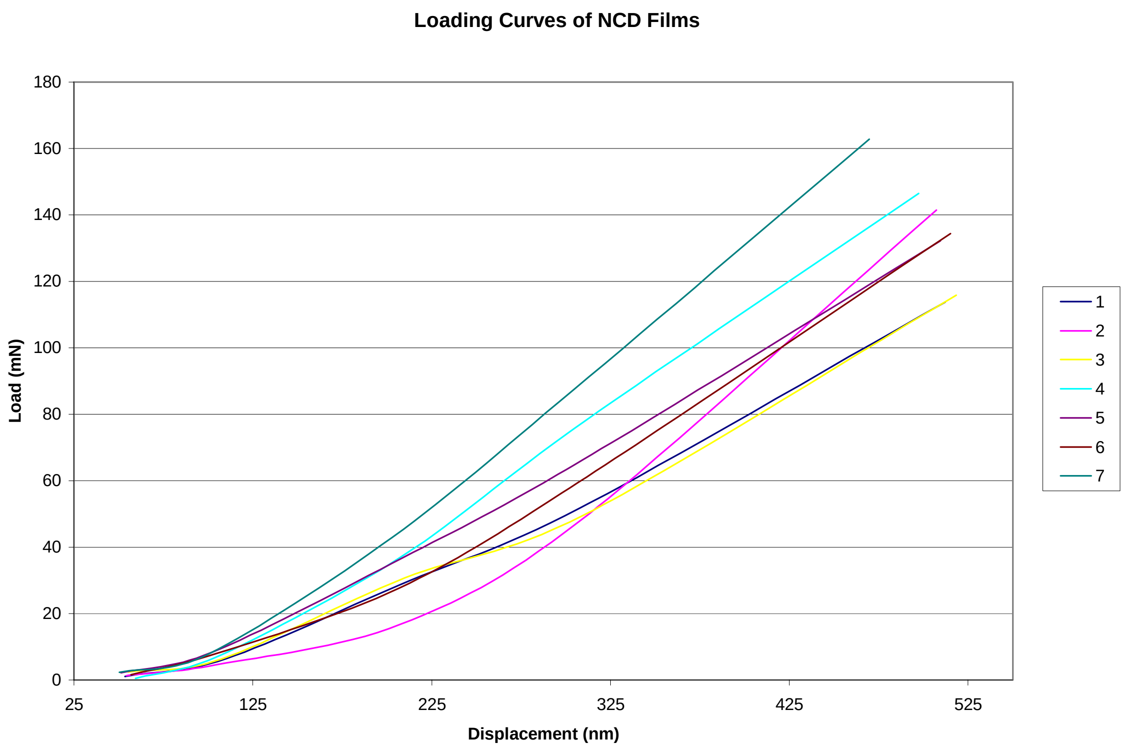

Fig 17. Loading Curves of NCD Films

Table 5. Hardness and Elastic Modulus of nanocrystalline diamond coatings

MATERIAL	**HARDNESS (GPa)**	**YOUNG'S MODULUS (GPa)**
1	29.4 ± 11.9	346.4 ± 98
2	45.7 ± 15.5	403.3 ± 76.9
3	33.9 ± 11.3	300.7 ± 39.9
4	54.3 ± 19.9	431.1 ± 107.9
5	47.7 ± 8.8	335.4 ± 36.6
6	47.3 ± 10.1	332.8 ± 46.6
7	72.0 ± 10.7	551.8 ± 71.5
Bulk Diamond [1]	120	1200
MPCVD NCD [19]	39.7 ± 2.2	387 ± 17
MPCVD NCD [29]	≈ 80	≈ 800
Titanium alloys	≈ 0.9	≈ 68.9

Hardness and elastic modulus of the nanocrystalline diamond coatings were determined by nanoindentation using a Nanoindenter XP® system. The maximum indentation depth was approximately 515 nm which is less than a third of the thinnest coating tested. Substrate properties did not affect the mechanical data extracted from this test. The hardness of these films ranged from 29.4 ± 11.9 GPa to 72.0 ± 10.7 GPa. While the indentation modulus varied between 346.4 ± 98 and 551.8 ± 71.5. Large errors are observed for both hardness and indentation modulus values. These errors can be ascribed to the surface roughness of the nanocrystalline diamond coatings. The extent of variation in the hardness and Young's modulus of the coatings is a direct result of the composition i.e. the relative quantities of nanocrystalline diamond, amorphous carbon and crystalline graphite. Coatings that contain larger deposits of graphite and amorphous carbon tend to be softer than those with high nanocrystalline diamond content.

The hardness and Young's modulus of a material attests to its ability to resist wear in harsh conditions. This ability is especially important for biomedical implants when considering wear particles could lead to serious medical complications such as hemorrhaging and internal clotting. The absolute values for the hardness of our NCD diamond coating compared favorably to NCD films characterized by Kuslich *et al.* [19] (39.7 ± 2.2 GPa) and Fries *et al.* [29] (80 GPa) but poorly with natural diamond (120 GPa). It is evident that nanocrystalline diamond films would also be useful to protect the surface of materials such as titanium alloys (0.9 GPa) from abrasion. These alloys are frequently implanted into the body coated with an oxide layer to prevent corrosion.

4.3 Scratch Adhesion Testing

Micro scratch tests were performed on the nanocrystalline diamond films to establish functional adhesion strength between the diamond film and the silicon substrate on which it is grown. These micro scratch tests also illustrate the failure mechanism for these coating systems. Though this is a simple test, the results are critical in determining the integrity of a coating/substrate system. The scratch path was recorded using optical microscopy during the test. The images obtained are shown below for the nanocrystalline diamond films (Fig. 18-23).

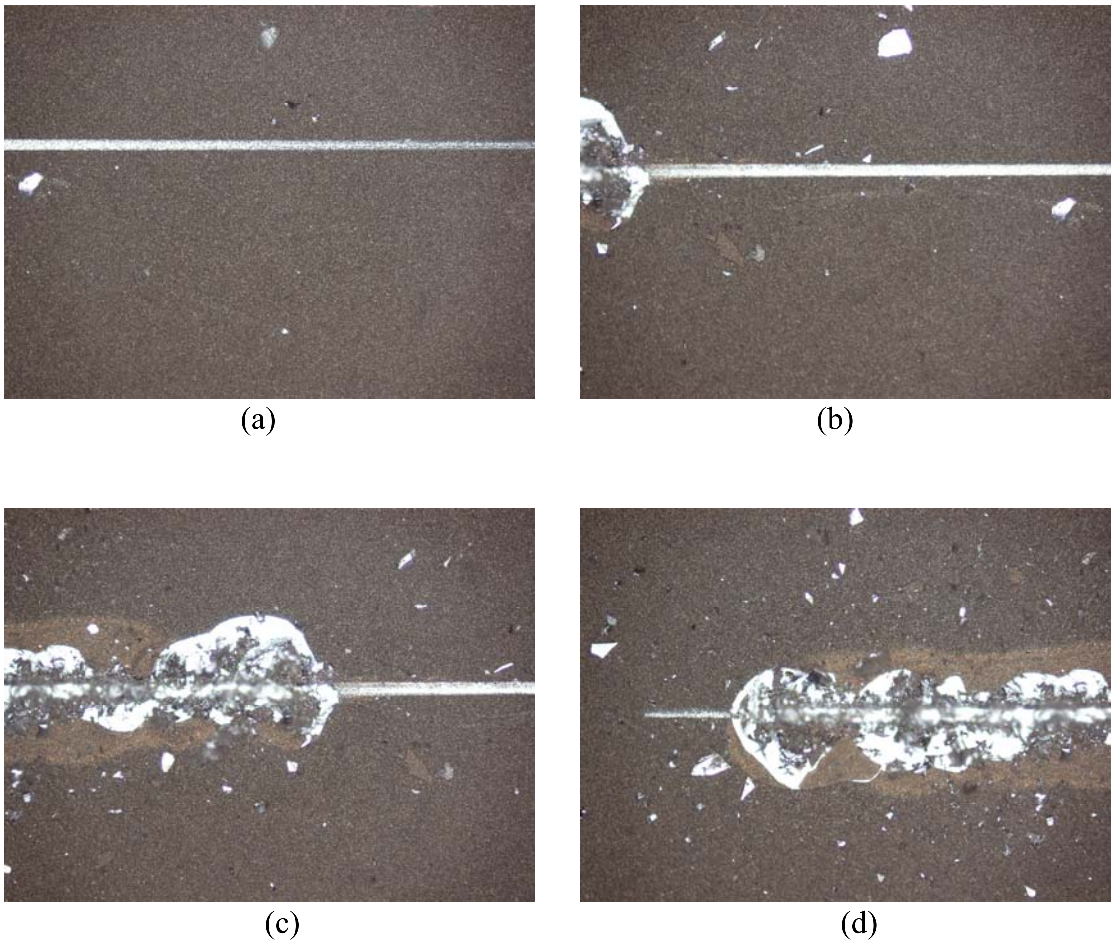

Fig. 18. Images showing scratch track of diamond tip – Sample 1 at different time frames; beginning of scratch test (a), intermediary phases showing damage as critical load is reached (b) and (c); end of scratch test (d). The load is increased linearly from the right to left.

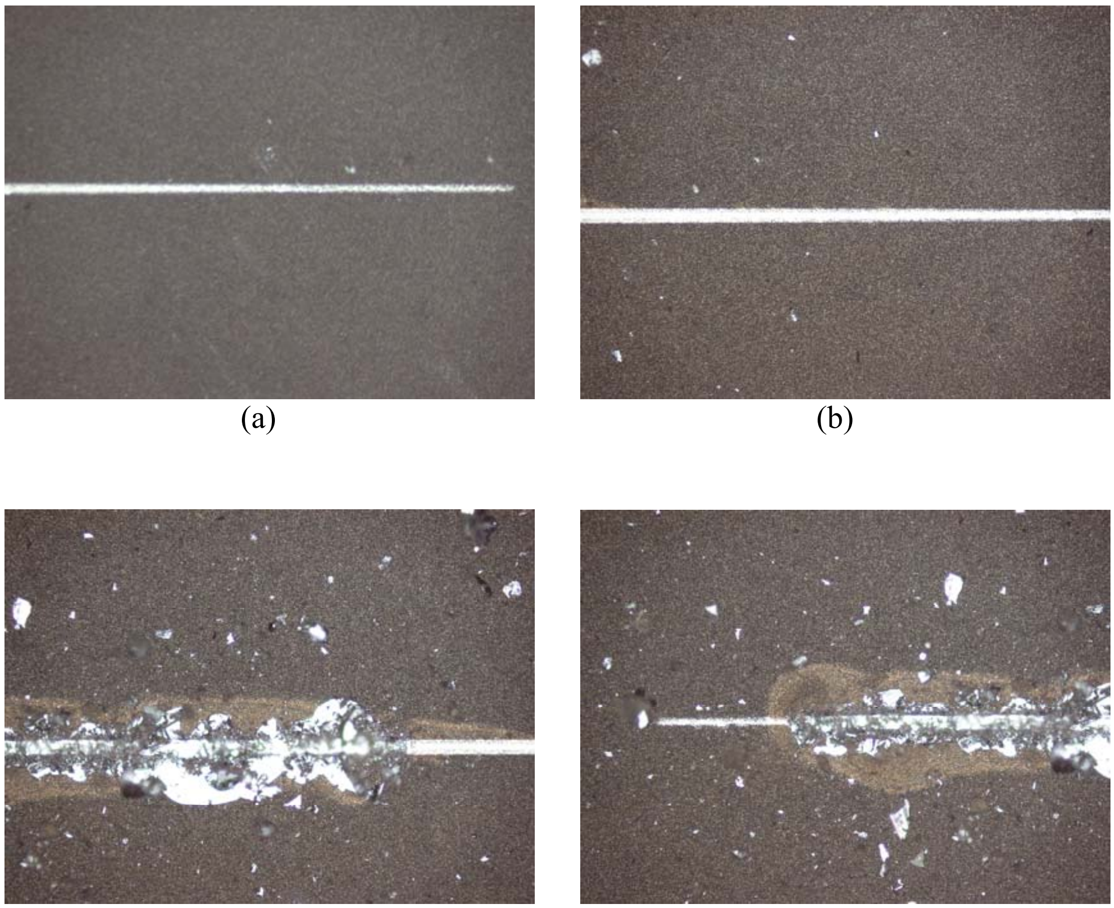

(a) (b) (c) (d)

Fig. 19. Images showing scratch track of diamond tip – Sample 2 at different time frames; beginning of scratch test (a), intermediary phases showing damage as critical load is reached (b) and (c); end of scratch test (d). The load is increased linearly from the right to left.

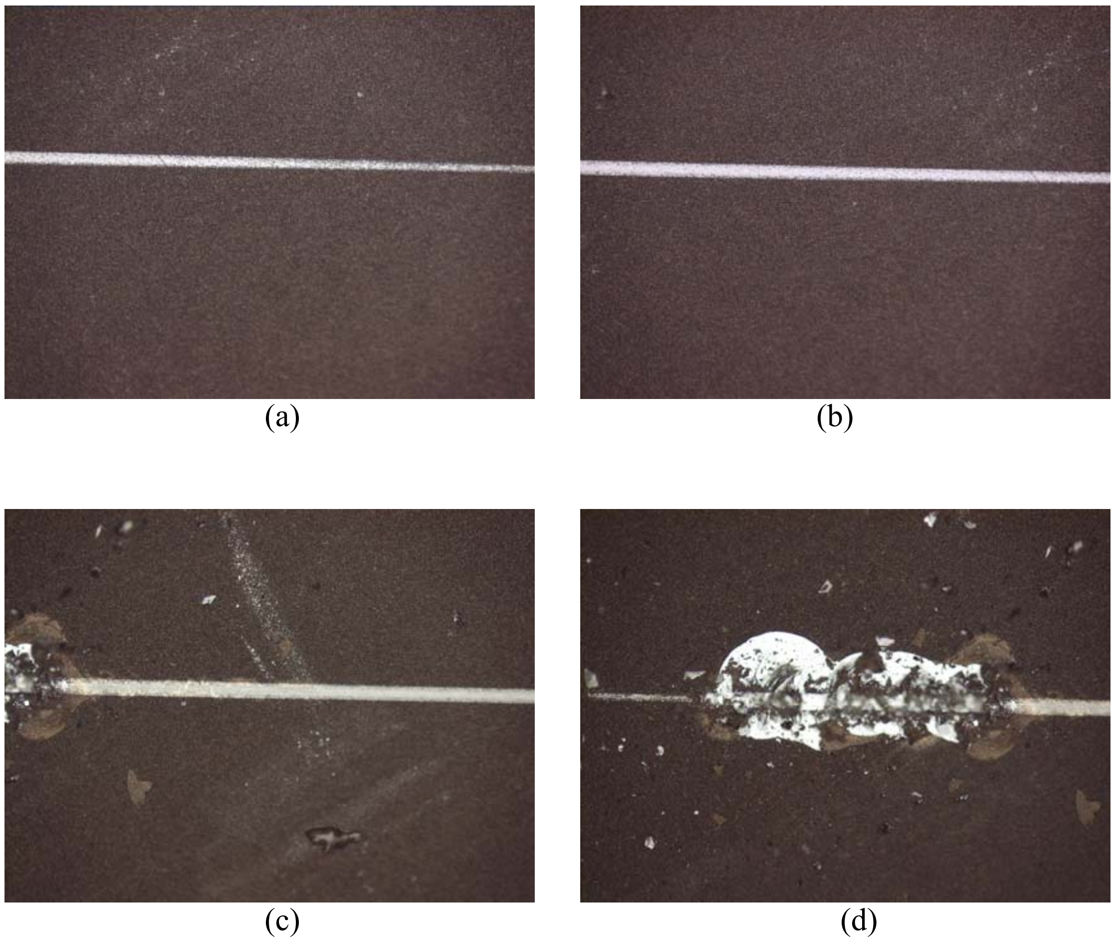

Fig. 20. Images showing scratch track of diamond tip – Sample 3 at different time frames; beginning of scratch test (a), intermediary phases showing damage as critical load is reached (b) and (c); end of scratch test (d). The load is increased linearly from the right to left.

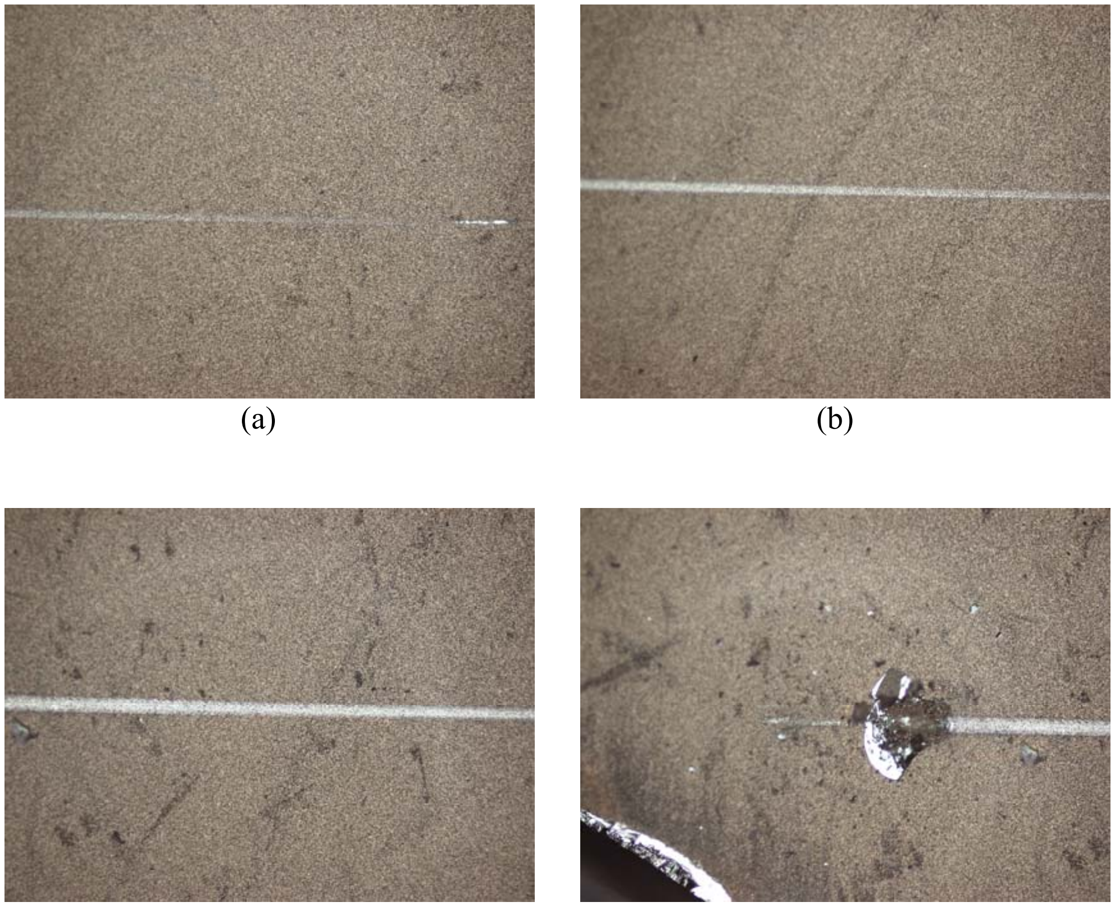

(a) (b)

(c) (d)

Fig. 21. Images showing scratch track of diamond tip – Sample 4 at different time frames; beginning of scratch test (a), intermediary phases showing damage as critical load is reached (b) and (c); end of scratch test (d). The load is increased linearly from the right to left.

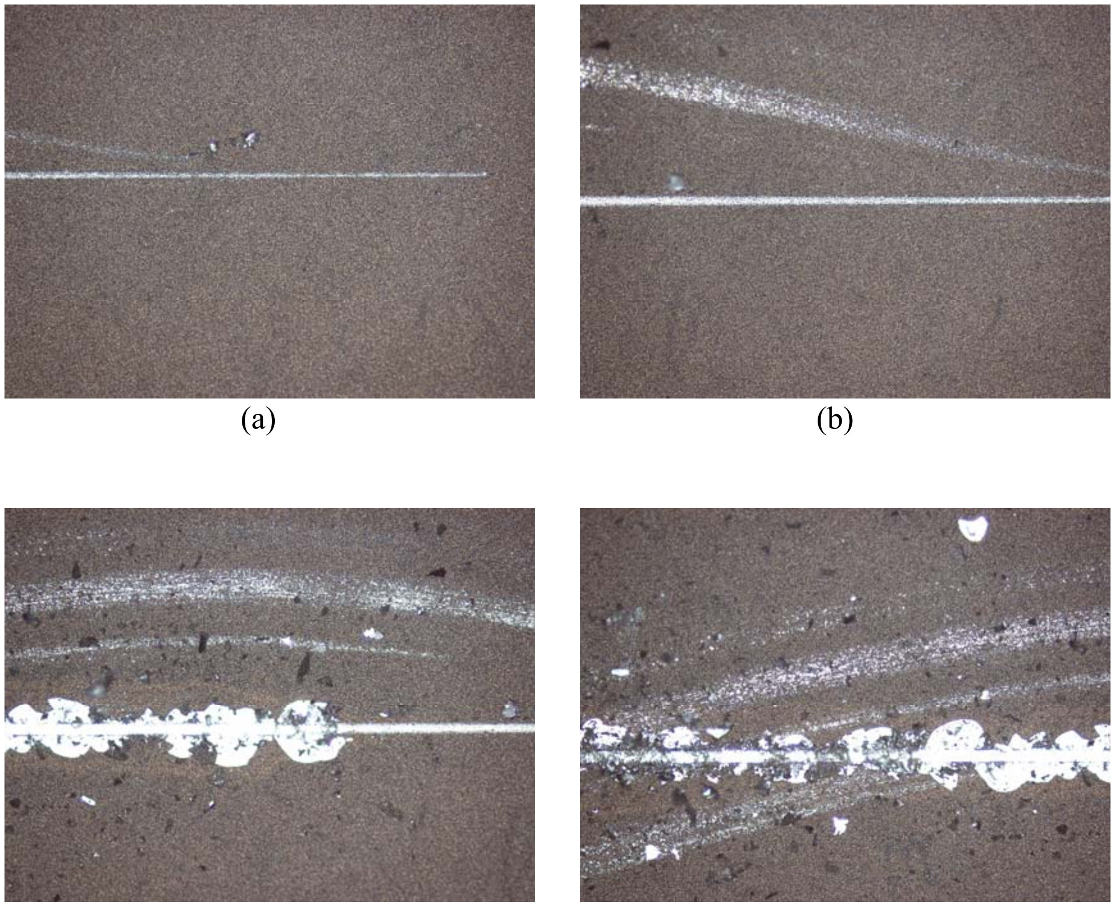

(a) (b) (c) (d)

Fig. 22. Images showing scratch track of diamond tip – Sample 6 at different time frames; beginning of scratch test (a), intermediary phases showing damage as critical load is reached (b) and (c); end of scratch test (d). The load is increased linearly from the right to left.

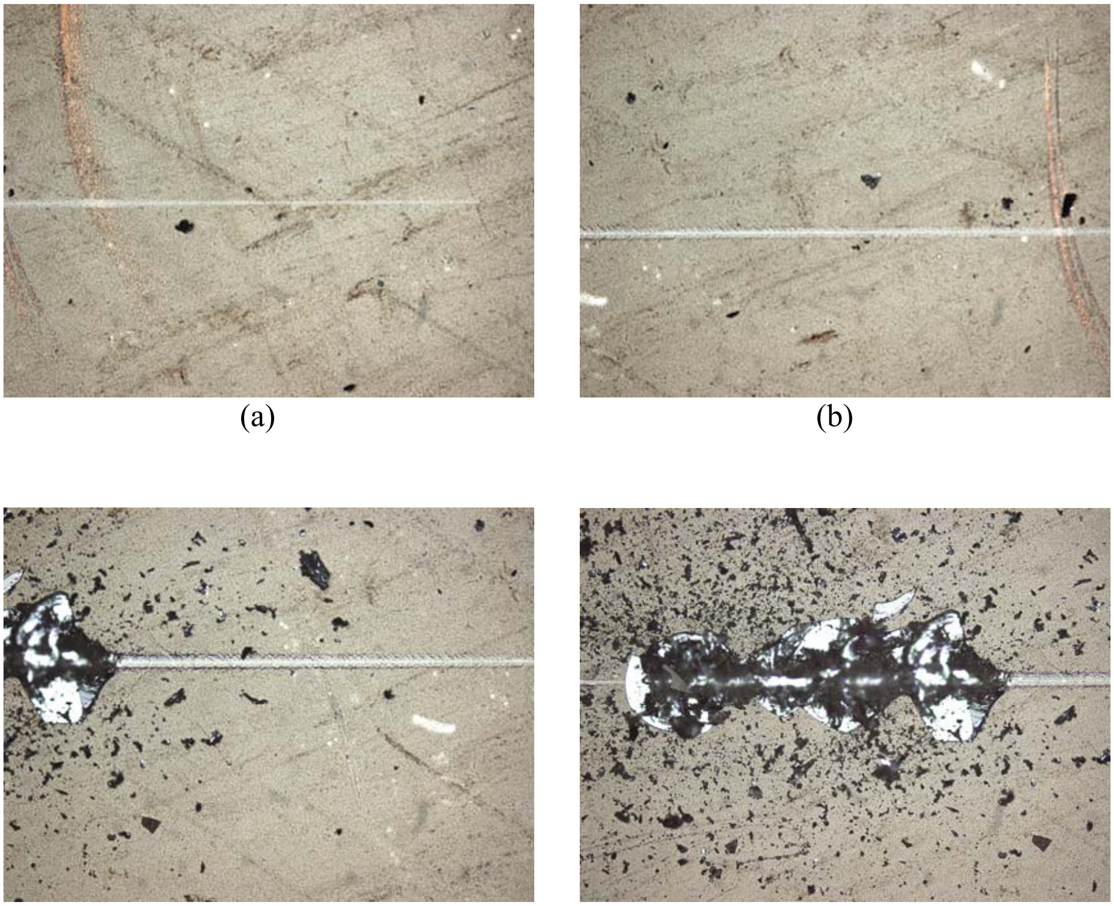

(a) (b) (c) (d)

Fig. 23. Images showing scratch track of diamond tip – Sample 7 at different time frames; beginning of scratch test (a), intermediary phases showing damage as critical load is reached (b) and (c); end of scratch test (d). The load is increased linearly from the right to left.

The nanocrystalline diamond/ silicon wafer systems displayed very good film adhesion. The critical load values at which the coatings delaminate are not reported due to the large error registered during the micro scratch tests. This is attributed to the surface roughness of the sample which causes the stylus to often jump and skip resulting in large fluctuations in force being applied normally onto the coating. However, we can estimate the critical loads based on the point at which the coating fails along the scratch path, the initial load applied and the rate of increase of the normal load [33].

$$L_{CN} = [L_{rate} * (l_n / X_{rate})] + L_{start} \qquad \text{Eq.(11)}$$

where L_{CN} = the critical scratch load in Newtons for a defined type of damage (Type N)

L_{rate} = the rate of force application (Newtons/minute) in the specific scratch test

l_n = the distance in millimeters between the start of the scratch track and the start point of the defined type of damage in the scratch track

X_{rate} = the rate of horizontal displacement (millimeters/minute) in the specific scratch test.

L_{start} = the preload stylus force in Newtons established at the start of the scratch test

Based on this calculation, the critical loads at which the mechanical integrity of these coatings fail vary from 3.1 – 3.4 N. The relatively high mechanical integrity observed is due to mechanical interlocking and chemical bonding between C and Si at the top layers of the substrate. Compressive stresses within the coating/ substrate system result from the applied normal and derived tangential forces. Consequently, plastic deformation of both the coating and the substrate occur producing tensile and conformal cracking followed by predominant buckling/ spallation failure of the coating. It is also important to note that cracking and buckling does not result in delamination or mechanical failure at locations away from the scratch site.

4.4 Bacterial Adhesion

Our primary objective was to evaluate the colonization of antimicrobial organisms on nanocrystalline diamond films. Hence, we utilized a CDC biofilm reactor (CBR) to incubate and grow *Psedomonas fluorescens*, gram negative bacteria, on the surfaces of nanodiamond composite on silicon and stainless steel coupons. The CBR operating in a continuous flow mode is thought to administer stresses encountered *in vivo* better than conventional batch culture setups [34]. Coupon samples were removed from the reactor after 8 hrs and 24 hrs in chemostat mode (continuous flow). These coupons were evaluated for retention of bacteria by Acridine Orange Direct Counts [46]. Table 6 shows the densities of bacteria on these samples at 24 hrs (Time 2).

Table 6. Number of *P. Fluoroescens* adherent to surfaces of NCD films and Stainless Steel

SAMPLE ID	GRAIN SIZE (μm)	BACTERIAL DENSITES (# x 10^6 / cm^{-2})	STANDARD DEVIATION (# x 10^6 / cm^{-2})	% of control bacterial density
2	0.60	24.0 ± 8.6	19.3	32.1
3	0.59	24.0 ± 8.6	19.3	32.1
4	0.06	6.1 ± 2.9	9.2	8.2
5	0.17 x 0.5	28.7 ± 2.9	9.3	38.4
6	0.47	39.2 ± 5.9	17.7	52.4
7	0.0628	51.5 ± 11.7	28.8	68.8
Control (Stainless Steel)	-	74.8 ± 20.3	40.6	100

The results in Table 6 illustrate that *P. fluorescens* easily colonizes the stainless steel control coupon as anticipated [50]. Nanocrystalline diamond films are less hospitable to the microorganisms. The number of cells detected on NCD films was as much as 68% less than that seen on the stainless steel control. However, the colonization of the NCD films is still quite significant. For sample 7, we observed the cell density to be $51.5 \pm 11.7 \times 10^6 / \text{cm}^{-2}$ after only 24 hours. At such high densities, bacteria can easily proliferate further in its protective biofilm and spread throughout the body. Consequently, we cannot confidently confirm that nanocrystalline diamond films reduce bacterial adhesion. No correlation between nanocrystalline diamond grain size and bacterial adhesion could be inferred. The results varied widely from film to film irrespective of the grain size or film morphology.

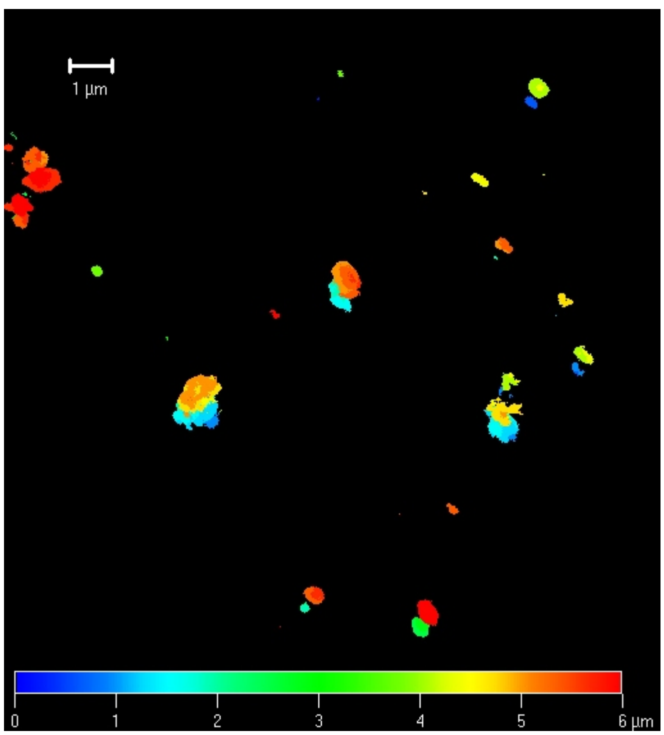

Fig. 24. Laser scanning confocal microscopy showing bacterial settlement

Bacterial infections of implanted medical parts continue to plague and frustrate patients in hospitals all around the world. Conventional methods of treating this affliction have been largely ineffective and have only served to make bacterial strains more robust [20, 36]. As such, novel strategies that combat the microbial pathogens at their site of infection are being introduced as the most viable biomedical solution. These methods include local drug delivery packages that dispense bioactive drugs at the site of implantation for instance the sustained-release system of vancomycin (VCM) using poly-L-lactide-co-caprolactone (PLCA) by Hirose *et al.* [3].

The second stratagem involves the immobilization of either antibiotic molecules or anti-biofouling moieties on biocompatible coatings. *In vitro* studies and a small number of *in vivo* investigations have shown that these approaches could be successfully applied in mammalian tissues to reduce bacterial infection associated with medical implants. However, they each have disadvantages which still make them susceptible to contamination and are too unsafe for trials in human patients. The necessity for the development of antibacterial coatings still persists; thus we investigated the antibacterial properties of nanocrystalline diamond coatings.

Nanodiamond films have received much attention recently due to their extraordinary physical and mechanical properties [11, 12, 13]. Narayan *et al.* [14] and Okroj *et al.* [17] suggested that this medium could be used to confer wear resistance and smoothness to biomedical implants such as cardiovascular assist devices and hip implants since they proved to be biocompatible and thromboresistive. One persistent problem with these devices is their high rate of bacterial infection after implantation. The antimicrobial nature of nanocrystalline diamond coatings was tested as a means of reducing this high rate of bacterial infection after implantation.

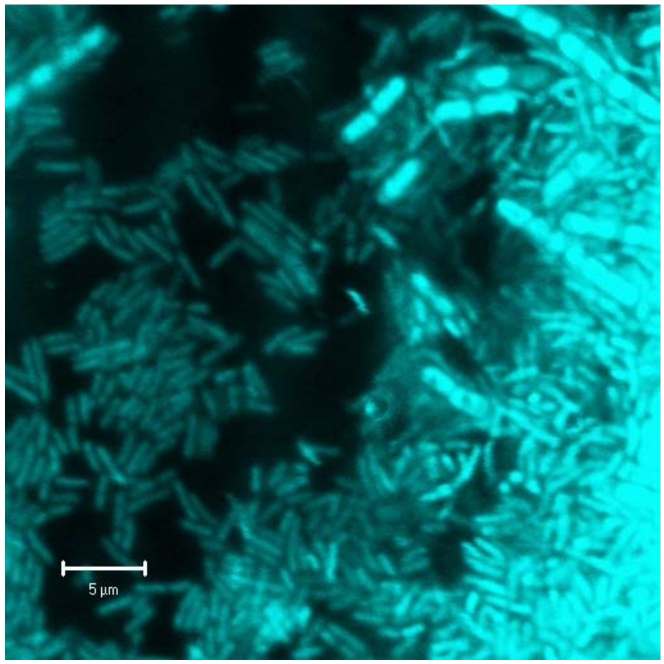

Fig. 25. Image of DAPI-stained *P. Fluorescens* on NCD film

Our results indicate that nanocrystalline diamond films are susceptible to colonization by bacteria. Quantitative data clearly shows that bacterial settlement on NCD films is quite significant and almost comparable to habitation of stainless steel by these pathogens. Stainless steel is known for its susceptibility to bacterial infection in patients [50]. Consequently, we can conclude that nanocrystalline films, a good candidate for biomedical coatings (based on biological properties), is prone to bacterial infection. The failure of this material to inhibit bacterial proliferation stands as testimony to the microorganism's innate ability to rapidly produce extracellular polymeric substances and multiply, upon attachment to the substrate surface [27]. This phenomenon is so potent that even if initial adhesion of the pathogen is reduced, subsequent cell division of the primary colonizers still result well established colonies and infection. Hence, we suggest investigating the efficacy of a nanocrystalline diamond coating doped with a bioactive agent (e.g. silver, triclosan, gentamicin). This model may prove to have all the characteristics desired for such an application.

V. CONCLUSIONS

This study demonstrates that nanocrystalline diamond films, grown on silicon (100) substrate and relatively low temperatures by microwave plasma enhanced chemical vapor deposition, have potential as biomedical implant coatings. Raman Spectroscopy, scanning electron microscopy and transmission electron microscopy confirmed the existence of nanocrystalline diamond in the thin films along with sp^2-hybridized carbon phases (amorphous carbon and graphite). Mechanical properties were analyzed using nanoindentation and micro scratch testing. From these tests, NCD films are shown to be quite hard and adhere closely with silicon (100) substrate. Bacterial inoculation in a rotating disk reactor proved that contrary to our hypothesis, nanocrystalline diamond surfaces are not resistant to bacterial colonization.

Future work will include more mechanical characterization in terms of directly examining the wear properties of these MPCVD nanocrystalline films. It will also be important to examine the antimicrobial properties NCD coatings doped bioactive moieties and their mechanical properties. Especially considering the physical, mechanical and biological properties nanocrystalline diamond films have been shown to exhibit.

VI. REFERENCES

[1] Pierson H. O., Handbook of Chemical Vapor Deposition. 1992, Park Ridge, New Jersey, USA: Noyes Publications

[2] Park J-H., Sudarshan T. S., Chemical Vapor Deposition. 2001, Ohio,, USA: ASM International.

[3] Hirose K., Marui A., Arai Y., Nomura T., Inoue S., Kaneda K., Fujita M., Komeda M. *Sustained-release vancomycin sheet may help to prevent prosthetic graft methicillin-resistant Staphylococcus aureus infection*. J. Vasc. Surg., 2006. 44: p. 377-382

[4] James N. R., Jayakrishnan A. *Surface thiocyanation of plasticized poly(vinyl chloride) and its effect on bacterial adhesion*. Biomaterials, 2003. 24: p. 2205-2212

[5] Bryers J. D., Jarvis R. A., Lebo J., Prudencio A., Kyriakides T. R., Uhrich K. *Biodegradation of poly(anhydride-esters) into non-steroidal anti-inflammatory drugs and their effect on Pseudomonas aeruginosa biofilms in vitro and on foreign-body response in vivo*. Biomaterials, 2006. 27: p. 5039-5048

[6] Speranza G., Gotardi G., Pederzolli C., Lunelli L., Canteri R., Pasquardini L., Carli E., Lui A., Maniglio D., Brugnara M., Anderle M. *Role of chemical interactions in bacterial adhesion to polymer surfaces*. Biomaterials, 2004. 25: p. 2029 – 2037

[7] Rojas I. A., Slunt J. B., Grainger D. W. *Polyurethane coatings release bioactive antibodies to reduce bacterial adhesion*. J. Con. Rel., 2000. 63: p. 175 – 189

[8] Tsibouklis J., Stone M., Thorpe A., Graham P., Peters V., Heerlien R., Smith J. R., Green K. L., Nevell T. *Preventing bacterial adhesion onto surfaces: the low-surface-energy approach*. Biomaterials, 1999. 20: p. 1229-1235.

[9] Tang H., Wang A., Liang X., Cao T., Salley S., McAllister J. P., Simon Ng K.Y. *Effect of surface proteins on Staphylococcus epidermis adhesion and colonization on silicone*. Colloids and Surfaces B: Biointerfaces, 2006. 51: p. 16-24

[10] Schierholz J. M., Steinhauser H., Rump A. F. E., Berkels R., Pulverer G. *Controlled release of antibiotics from biomedical polyurethanes: morhphological and structural features*. Biomaterials, 1997. 18:p. 839-844

[11] Gruen D. M. *Nanocrystalline diamond films*. Annu. Rev. Mater. Sci., 1999. 29: p. 211-259

[12] Abreu C.S., Amaral M. S., Oliveira F. J., Tallaire A., Benedic F., Syll O., Cicala G., Gomes J. R., Silva R. F. Tribological testing of self-mated nanocrystalline diamond coatings on Si_3N_4 ceramics. Surface and Coatings Technology, 2006. 200: p. 6235-6239

[13] Kvasnica S., Schalko J., Bernardi J., Vorlaufer G., Pauschitz A., Roy M. Nanotribological study of PECVD DLC and reactively sputtered Ti containing carbon films. Diamond and Related Materials, 2006. 15: p. 1743 - 1752

[14] Narayan R. J., Wei W., Jin C., Andara M., Agarwal A., Gerhardt R. A., Shih C., Shih C., Lin S., Su Y., Mamedov S., Boolchand P., Ramamurti R., Singh R. N. *Microstructural and biological properties of nanocrystalline diamond coatings*. Diamond and Related Materials, 2006.

[15] Mitura K., Niedzielski P., bartosz G., Moll J., Walkowiak B., Pawlowska Z., Louda P., Kiec-Swierczynska M., Mitura S. *Interactions between carbon coatings and tissue.* Surface and Coatings Technology, 2005.

[16] Mitura s., Mitura A., Niedzielski P., Couvrat P. *Nanocrystalline Diamond Coatings*. Chaos, Solitons and Fractals, 1999. 10 (12): p. 2165 – 2176

[17] Okroj W., Kaminska M., Klimek L., Szymanski W., Walkowiak B. *Blood platelets in contact with nanocrystalline diamond surfaces*. Diamond and Related Materials, 2006. 15: p. 1535-1539

[18] Garguilo J. M., Davis B. A., Buddie M., Kock F. A. M., Nemanich R. J. *Fibrinogen adsorption onto microwave plasma chemical vapor deposited diamond films*. Diamond and Related Materials, 2004. 13: p. 595-599

[19] Kulisch W., Popov C., Vorlicek V., Gibson P. N., Favaro G. *Nanocrystalline diamond growth n different substrates*. Thin Solid Films, 2006.

[20] Darouiche R. O. *Antimicrobial approaches for preventing infections associated with surgical implants*. Healthcare Epidemiology, 2003. 36: 1284 – 1289

[21] Cerca N., Pier G. B., Vilanova M., Oliveira R., Azeredo J. *Quantitative analysis of adhesion and biofilm formation on hydrophilic and hydrophobic surfaces of clinical isolates of Staphylococcus epidermis*. Research in Microbiology, 2005. 156: p. 506 – 514

[22] Planchon S., Gaillard- Martinie B., Dordet-Frisoni E., Bellon-Fontaine M. N., Leroy S., Labadie J., Hebraud M., Tallon R. *Formation of biofilm by Staphylococcus xylosus*. Int. J. Food Microbio., 2006. 109: p. 88-96

[23] Baumgartner J. N., Cooper S. L. *Influence of thrombus components in mediating staphylococcus aureus adhesion to polyurethane surfaces*. J. Biomed. Mater. Res., 1998. 40: p. 660-670

[24] Miron J., Ben-Ghedalia D., Morrison M. *Adhesion mechanisms of rumen cellulolytic bacteria.* J. Dairy Sci., 2001. 84: p. 1294-1309

[25] Girard V., Mourez M. *Adhesion mediated by autotransporters of Gram-negative bacteria: Structural and functional features*. Research in Microbiology, 2006. 157: p. 407-416

[26] Hussain S., Roy R. K., Pal A. K. *Incorporation of silver nanoparticles in DLC matrix and surface plasmon resonance effect.* Materials Chemistry and Physics, 2006. 99: p. 375 – 381.

[27] Rickard A.H., Gilbert P., High N. J., Kolenbrander P. E., Handley P. S. *Bacterial coaggregation: an integral process in the development of multi-species biofilms*. Trends in Microbiology, 2003. 11(2): p. 94 – 100

[28] Ramamurti R., Shanov V., Singh R. N., Mamedov S., Boolchand P. *Raman spectroscopy study of the influence of processing conditions on the structure of polycrystalline diamond films*. J. Vac. Sci. Technol., 2006. 24(2): p. 179 – 189

[29] Fries M. D., Vohra Y. K. *Properties of nanocrystalline diamond thin films grown by MPCVD for biomedical implant purposes*. Diamond and Related Materials, 2004. 13: p. 1740 -1743

[30] Gouldstone A., Chollacoop N., Dao M., Li J., Minor A. M., Shen Y. *Indentation across size scales and disciplines: Recent developments in experimentation and modeling*. Acta Materialia, 2006.

[31] Le Bourhis E., Patriarche G. *TEM-nanoindentation studies of semiconducting structures*. Micron, 2006.

[32] Oliver W. C., Pharr G. M. An improved technique for determining hardness and elastic modulus using load displacement sensing indentation experiments. J. Mater. Res., 1992. 7: 1564-1583

[33]Gonczy S. T. Adhesion Strength and Mechanical Failure Modes of Ceramic Coatings by Quantitative Single Point Scratch Testing. Gateway Materials Technology.

[34] Goeres D.M., Loetterele L.R., Hamilton M. A., Murga R., Kirby D. W., Donlan R. M. Statistical assessment of a laboratory method for growing biofilms. Microbiology, 2005. 151: p. 757-762

[35] Flemming R. G., Capelli C. C., Cooper S. L., Proctor R.A. *Bacterial colonization of functionalized polyurethanes*. Biomaterials, 2000. 21: p. 273-281

[36] Rice L. B. *Unmet medical needs in antibacterial therapy*. Biochemical Pharmacology, 2006. 71: p. 991-995

[37] Morrison M. L., Buchanan R. A., Liaw P. K., Berry C. J., Brigmon R. L., Riester L., Abernathy H., Jin C., Narayan R. J. *Electrochemical and antimicrobial properties of*

diamondlike carbon-metal composite films. Diamond and Related Materials, 2006. 15: p. 138-146

[38] Narayan R. J., Berry C. J., Brigmon R. L. *Structural and biological properties of nanotube composite films*. Materials Science and Engineering, 2005. B123: p. 123 -129.

[39] Danese P. N. *Antibiofilm approaches: prevention of catheter colonization*. Chem. & Bio., 2002. 9: p. 873-880

[40] Raad I., Hachem R., Zermeno A., Dumo M., Bodey G. P. *In vitro antimicrobial efficacy of silver iontophorectic catheter*. Biomaterials, 1996. 17: p. 10055- 1059

[41] Oloffs A., Grosse-Siestrup C., Bisson S., Rinck M., Rudolph R., Gloss U. *Biocompatibility of silver-coated polyurethane catheters and silver-coated Dacron material*. Biomaterials, 1994. 15 (10): p. 753 – 758

[42] Balazs D. J., Triadafillu K., Wood P., Chevolot Y., van Delden C., Harms H., Hollenstein C., Mathieu H. J. *Inhibition of bacterial adhesion on PVC endotracheal tubes by RF-oxygen glow discharge, sodium hydroxide and silver nitrate treatments*. Biomaterials, 2004. 25: p. 2139-2154

[43] Schierholz J. M., Lucas L. J., Rump A., Pulverer G. *Efficacy of silver-coated medical devices*. J. Hospital Infection, 1998. 40: p. 257-262

[44] Woo G. L. Y., Mittelman M. W., Santerre J. P. *Synthesis and characterization of a novel biodegradable antimicrobial polymer*. Biomaterials, 2000. 21: p. 1235 – 1246

[45] Sun C., Zhang W. J., Lee S., Bello I., Lee S. T. *Nucleation of diamond films by ECR-enhanced microwave plasma chemical vapor deposition*. Diamond and Related Materials, 1999. 8(8-9): p. 1410-1413

[46] Brigmon, R.L., M. M. Franck, J. S. Bray, S. Lanclos, D. Scott, and C. B. Fliermans. *Direct immunofluorescence and enzyme-linked immunosorbent assays for evaluating organic contaminant degrading bacteria*. J. Microbiol. Methods, 1998. 32: p.1-10.

[47] Kastner, J. R., J Santo Domingo, M Denham, M Molina, R Brigmon. *Effect of Chemical Oxidation on Subsurface Microbiology and Trichloroethylene (TCE) Biodegradation.* Bioremediation J., 2000. 4: p. 219-236.

[48] Vouagner D., Champagnon B., Snidero E., Tromson D., Bergonzo P. and Girardeau-Montaut J. P. *Photoemission properties and hydrogen surface coverage of CVD diamond films*. Diamond and Related Materials, 2004. 13: p. 969-974

[49] Ikeda R., Tanei H., Nakamura N., Ogi H., Hirao M., Sawabe A., Takemoto M. *Elastic constant of nanocrystalline diamond film*. Diamond and Related Materials, 2006. 15: p. 729 – 734.

[50] Bosetti M., Massè A., Tobin E., Cannas M. *Silver coated materials for external fixation devices: in vitro biocompatibility and genotoxicity*. Biomaterials, 2002. 23(3): p. 887-892.

APPENDIX

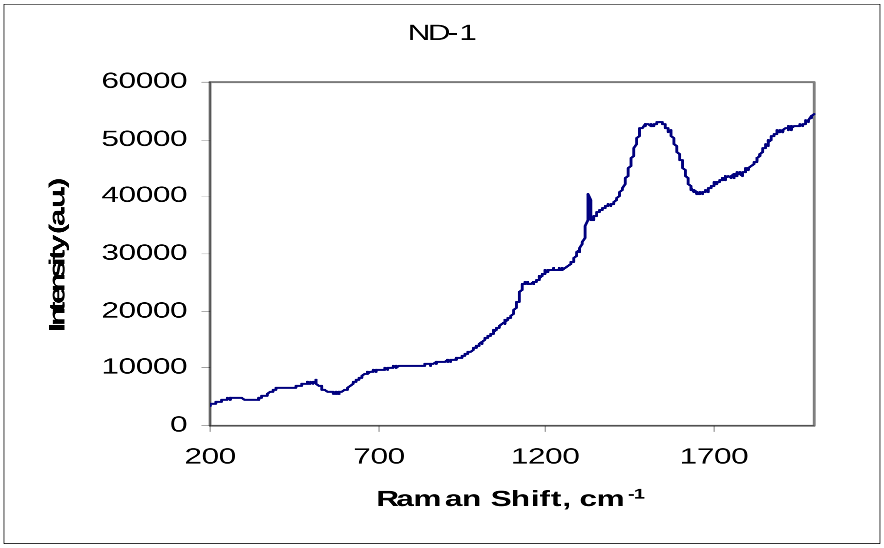

Fig. 26. Raman Spectra of nanocrystalline diamond – Sample 1

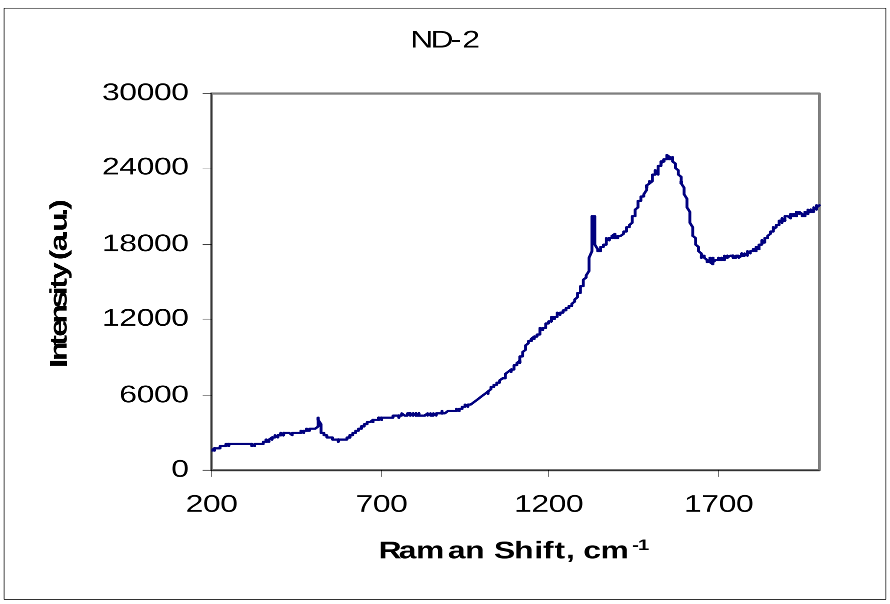

Fig. 27. Raman Spectra of nanocrystalline diamond – Sample 2

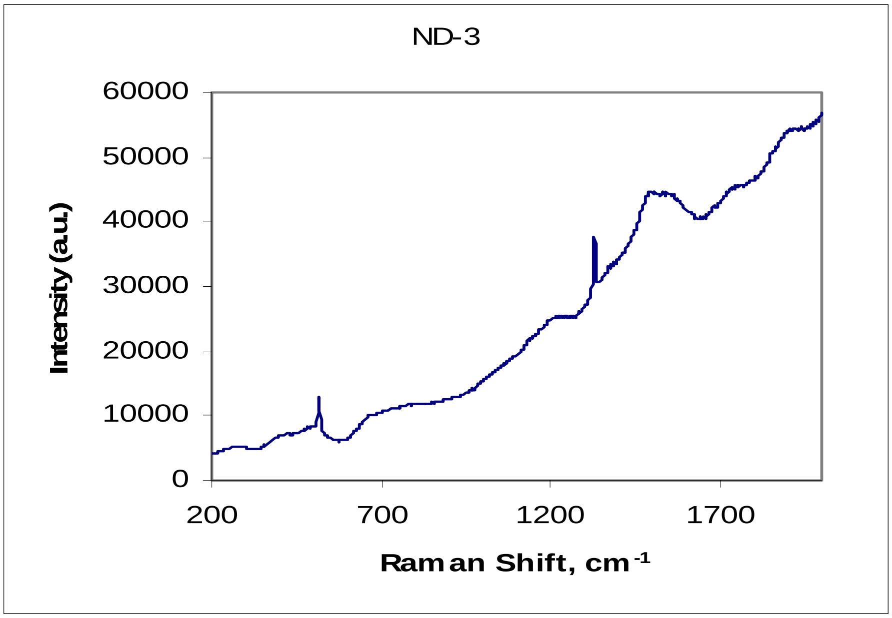

Fig. 28. Raman Spectra of nanocrystalline diamond – Sample 3

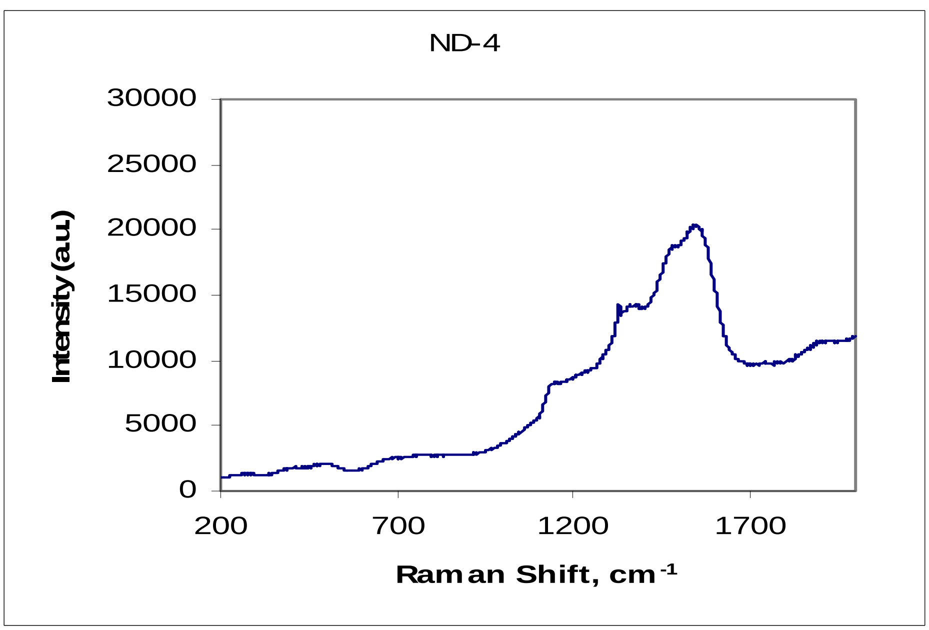

Fig. 29. Raman Spectra of nanocrystalline diamond – Sample 4

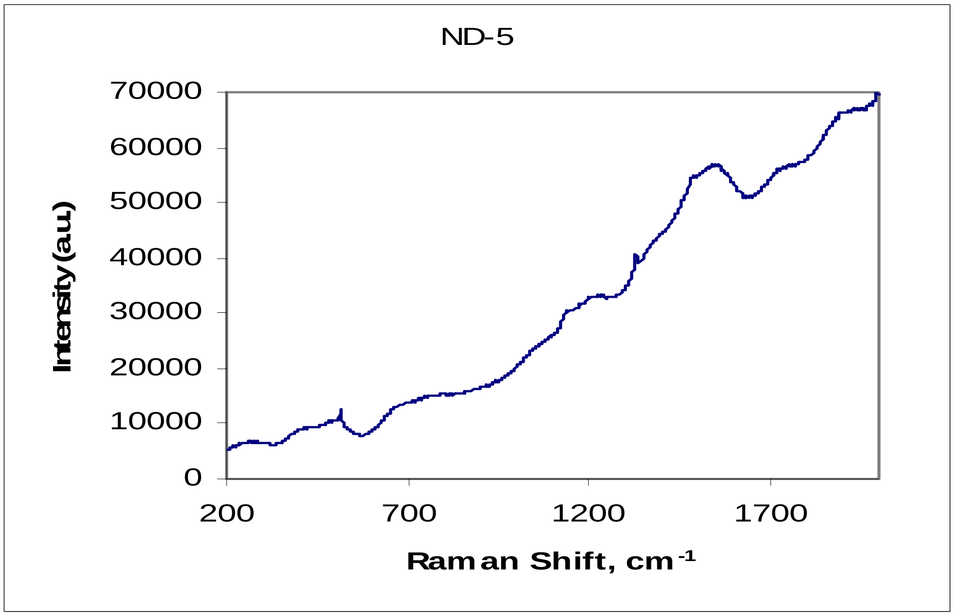

Fig. 30. Raman Spectra of nanocrystalline diamond – Sample 5

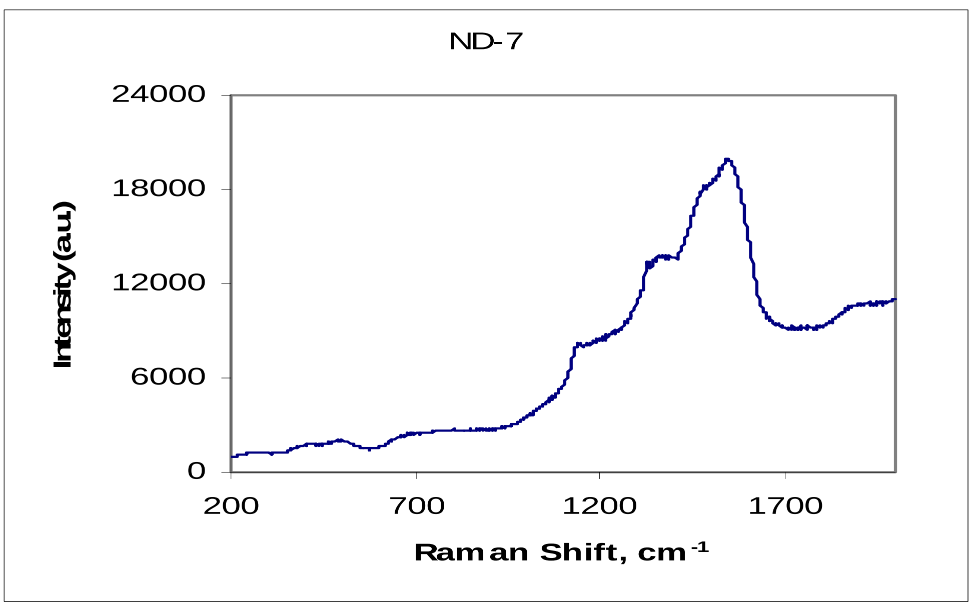

Fig. 31. Raman Spectra of nanocrystalline diamond – Sample 7